CHARGE EXCHANGE OF K$^+$

ON PLATINUM AT THREE GEV/C

by

GEORGE FITZGERALD SMOOT III

S.B., Massachusetts Institute of Technology

(1966)

SUBMITTED IN PARTIAL FULFILMENT

OF THE REQUIREMENTS FOR THE

DEGREE OF DOCTOR OF

PHILOSOPHY

at the

MASSACHUSETTS INSTITUTE OF

TECHNOLOGY

February, 1971

Signature of Author _____

Department of Physics, September 17, 1970

Certified by _____

Thesis Supervisor

Accepted by _____

Chairman, Departmental Committee on

Graduate Students

CHARGE EXCHANGE OF K^+

ON PLATINUM AT THREE GeV/c

by

GEORGE FITZGERALD SMOOT III

Submitted to the Department of Physics on September 17, 1970, in partial fulfilment of the requirements for the degree of Doctor of Philosophy.

ABSTRACT

Data were taken for three GeV/c K^+'s incident on scintillator and platinum targets where a K^0 was observed as a reaction product. A model of these nuclei was made up assuming simple nuclear momentum distributions and independence of the nucleons from each other during interaction with kaons. The predictions of this model are compared with the measured data. The model appears to describe the data adequately.

Thesis Supervisor: David H. Frisch

Title: Professor of Physics

Table of Contents

List of Figures

I. Introduction

The purpose of this experiment was to observe the production of K^o's by three GeV/c K^+'s incident on a platinum target, in particular to measure the K^o's momentum and angular distribution, and to see if an adequate model could be found to predict these distributions.

There has been increasing use of nuclei other than hydrogen for the targets in high energy collision experiments. Specifically, this same platinum target configuration has been used for a test of $\Delta S = \Delta Q$ rule in K^o leptonic decay.

The problem of high energy hadron reactions with nuclei has a fairly long history, as deuterium has traditionally been the source of neutrons for experimenters who have wanted to use neutron targets. The experimenters' main concern was how to correct for the additional presence of a proton in order to measure the reaction free neutrons. The method generally used is the Glauber correction.[11]

The mechanics of the experiment was as follows: A 3.0 GeV/c K^+ beam was sent into a platinum target and the reaction products were detected by electronic counters and optical spark chambers. Specifically, the intent was to detect and observe the K^o's which decayed through $K_1^o \rightarrow \pi^+\pi^-$.
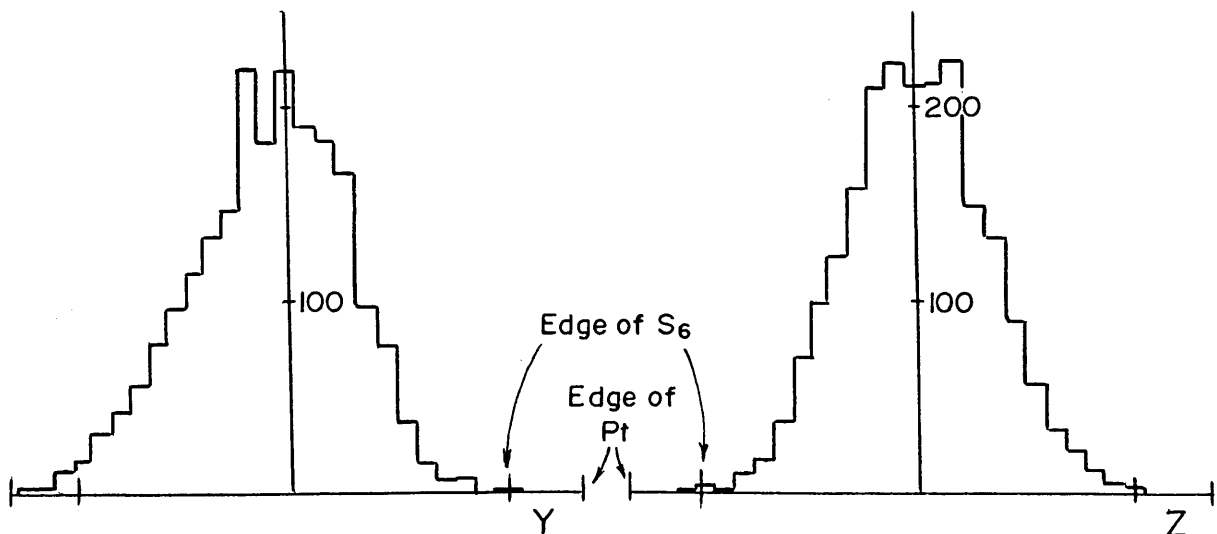
II. The Beam

The incident beam used in this experiment was designed by Dr. O. Fackler as a partially separated K^+ beam. The K^+'s in this beam were then used to produce a secondary K^o beam for a test of the $\Delta S = \Delta Q$ rule in $K^o \rightarrow \pi e \nu$ decay.

The reason for the title of "partially separated K^+ beam" is that the K^+'s were physically partially separated from the other particles produced by the internal proton beam of the Brookhaven Alternating Gradient Synchrotron colliding with an internal beryllium oxide target. This partial physical separation was accomplished by the beam transport system, which consisted of magnets, collimators, and electrostatic separators[1]. The end result was to be a nearly parallel two-inch diameter beam of 3.0 GeV/c π and K mesons incident on the platinum target.

In addition to the beam transport system there was an electronic system used to designate when a particle was present and whether it was a kaon or pion. The tagging was done by a beam telescope of scintillation and Čerenkov counters and some associated fast logic circuitry. (See Figure I for position and perspective of these counters.) These counters were, from upstream to downstream, S_2 and S_3, two scintillation counters, Č, a differential Čerenkov counter for electronically separating kaons and pions, S_4, another scintillation counter, V, a vetoing scintillation counter with a hole in the middle, and S_6, a scintillation counter located just in front of the platinum target.

How did this system work? Operating with uniform internal
proton beam spill of one-half second duration and 2×10^{12} protons
every 2 1/2 seconds, the beam was measured to be 20 to 25% K^+'s and
for a total flux of 60 to 80 thousand particles per spill it had two
particles overlapping the resolution of the spark chambers 8 to 10%
of the time. The curves of the Čerenkov counter Č (see Figure II)
imply that for every incident K^+ there are $\sim 10^{-4}$ π^+'s that are
accepted as K^+'s. This fact, coupled with the cross-section for
$\pi^+ + Pt \rightarrow K_1^o$ + others (< 1 barn) means that for the total flux of
the experiment there is expected to be less than one π^+ induced
event present in the data.

In addition to the beam telescope counters there were three
beam chambers (for a portion of the experiment there was only the
downstream or main beam chamber present) which were used to
measure the position of the beam particles more accurately. (Again
see Figure I.) The beam size was measured by observing the distribu-
tion of spark location in the main beam spark chamber.

The angular distribution of the beam was measured using the beam spark chambers and the momentum analysis chambers.

In the top view

Beam Slope   (milliradians)

Slope Resolution
between Momentum
Analysis & Beam
Spark Chambers

In the side view

Beam Slope   (milliradians)

Slope Resolution
between Momentum
Analysis & Beam
Spark Chambers
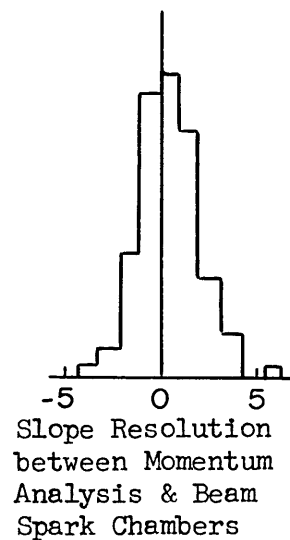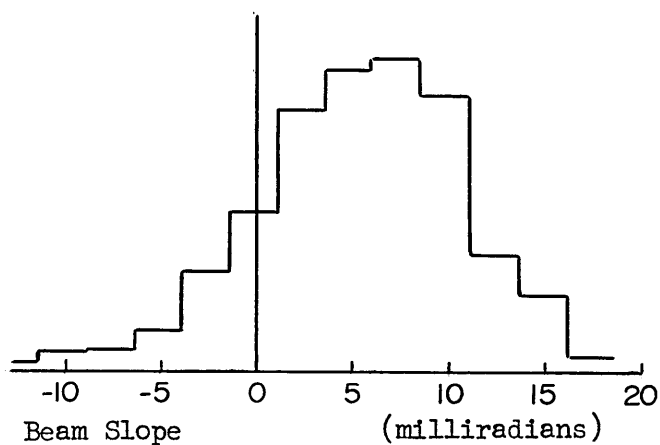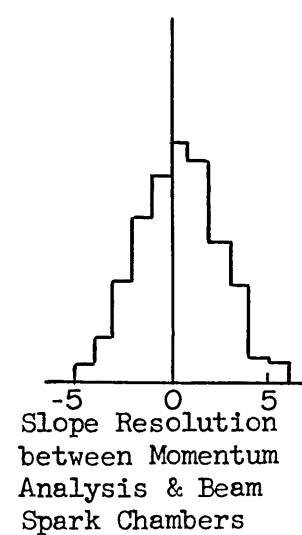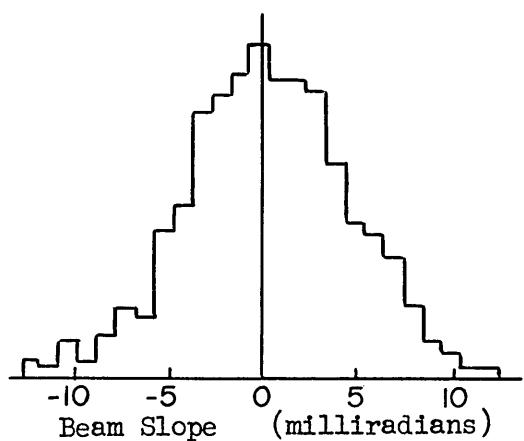
The angular divergence in the top view is what one would expect from the limits of the scintillation counters. The side

view angular divergence is less than that set by the scintillation counters; it appears to be set by the beam optics.

Next we come to the momentum of the beam. The beam was designed to have a central momentum of 3.0 GeV/c with a width of ± 1/2% or 15 MeV/c. By using the momentum analysis chambers the momentum of the beam was found to be 2.9 ± 0.1 GeV/c.

Beam Momentum (GeV/c)
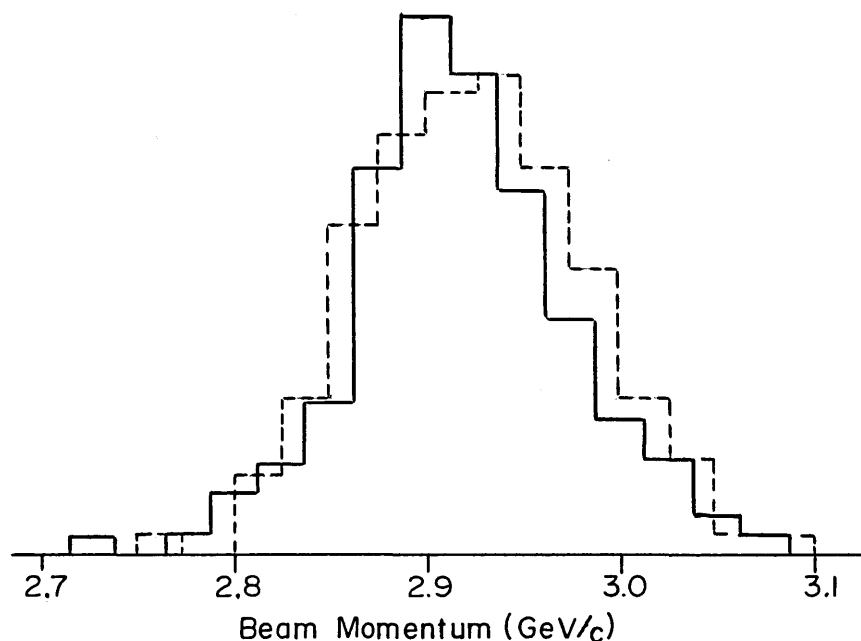
The beam chambers were located in the fringing field of the magnet, so the analysis of the momentum was not as simple as for the momentum analysis chambers which were located in a nearly homogeneous magnetic field; however, a rough map was made of the magnetic field in the beam entrance region. From this measurement a model was made of the magnetic field (see Figure III) and trajectories were calculated for 2.0 or 3.0 GeV/c particles (see Figure IV) with the magnet on and off.

As can be seen from Figure IV, these trajectories are approx-
imately straight lines through the first two beam chambers and only
really deviate from each other at the last chamber. One can use
this information to find the momentum of a beam particle by
extrapolating spark locations from the first two chambers and
finding the difference from the spark location in the main beam
chamber. This appears to be accurate to about ± 0.5 GeV/c. (See
Figure V.) The reason the data appear broader than the selected
momenta spectra is that the data often have less sparks in the beam
chamber and thus less accuracy than the selected events.

In summary one can say that all the observed interactions are
induced by K^+ mesons whose angles are known to ± 2 milliradians,
whose positions are known to ± 40 mils, and whose momentum is known
to ± 500 MeV/c (± 100 MeV/c to good assurance).

III. The Target

A. The Layout

The target was a cylinder of platinum 3.0 inches in diameter
and 2.0 centimeters thick. The platinum was borrowed from the
Atomic Energy Commission. Its composition was as follows:

ATOMIC NUMBER	NUMBER OF NEUTRONS	% NATURALLY OCCURRING
192	114	0.8
194	116	32.8
195	117	33.7
196	118	25.4
198	120	7.3

The intent of the experiment was to have the K^+ beam interact
with the platinum target and undergo the process of charge exchange.
In order to facilitate this process, the platinum target was
sandwiched between a 3/16 inch thick by 2 1/4 inch diameter
scintillation counter S_6 centered on the front face and a 3/8 inch
thick by 5 1/4 inch diameter scintillation counter centered on the
back face. See Figure VI for the configuration of this system.

The reason that the front counter S_6 was placed directly
adjacent to the target was that experience shows that if the last
counter is removed a reasonable distance from the target ($\sim$ a meter)
for every K^+ that undergoes charge exchange there will be a K^+ that

does not reach the target (e.g. one K^+ in two thousand decays in a
meter). However, when the scintillation counter is just in front of
the target, the beam chamber indicates that less than 0.1% of the
time is there no beam when one is indicated by the whole beam
telescope.

The scintillation counter behind the target was used on most
occasions to veto events which sent charged particles into it. This
counter was found to be better than 99.9% efficient in vetoing
charged particles passing through it when used in conjuction with
its special electronics. Immediately following this scintillation
counter was the first momentum analysis chamber.

B. Trigger Requirement

For data taken with the requirements of the beam telescope and
with the veto of charged particles by the downstream scintillation
counter, we have two limits as to where a K^o produced by a K^+ can
originate.

(1) The downstream end: A direct check of the momentum
analysis chambers shows that no K^o's were observed which
were produced downstream of the first gap of the first
momentum analysis chamber. In addition, due to the great
efficiency of the downstream scintillation counter, it is
probable that no more than the first quarter to third of
this counter could be the origin of those events.

(2) The upstream end: The efficiency of the differential

Čerenkov counter Č would imply that all K^+'s under
consideration made it to the center of Č. In addition,
S_4 and S_6 guarantee that a charged particle was seen by
both. Along with this electronic criterion the beam
chamber was required to have a track of reasonable
direction. It seems fair to expect all observed events
to have origins between the middle of the last beam
chamber and the first fraction of the veto counter.

C. Estimate of Relative Sources of K^o's

On the basis of total collision lengths, the platinum target
would appear as 94% of the matter present in this region. One
would expect the scintillation counters to make up most of the rest
of the sources, i.e. S_6 3% and the first fraction of the veto ~ 2%.
In order to investigate this hypothesis and to correct for the effect
of these and other sources, a set of data was taken without the
platinum in place. This was done by a series of data runs in which
various thicknesses of scintillator were in place of the platinum.
These data were extrapolated to zero thickness of S_6. The production
rate at zero thickness was calculated to be half that for S_6 with
the platinum removed.

This value is consistent with the estimates above in so far as
it is assumed that the platinum target does not have a major effect
on the interaction through such mechanisms as stopping low energy
charged particles or converting gamma rays. The absolute rate for

target removed was $\sim$ 4% of that for the target in place, which is
also consistent.

IV. Detection of the Reaction

A. Apparatus

For detection of the K^+ charge exchange on platinum, the apparatus shown in Figure I was used. Immediately behind the target was a scintillation counter which in turn was followed by eight momentum analysis spark chambers and a lead plate spark chamber. All of these were placed inside the Argo magnet, a region of nearly homogeneous vertical magnetic field. The spark chambers were of the optical type and were viewed through holes in the top pole piece located directly above the chambers and their 90° stereo mirrors. The eight momentum analysis chambers were made with four working gaps separated by one mil aluminum foil.

B. Electronic Selection of Events

In general, these spark chambers were triggered on the condition that the beam telescope had indicated that a K^+ had entered the target (called a K^+ trigger) or that in addition to this the scintillation counter behind the target indicated no charged particles had traversed it (called a K^o trigger). The spark images from the beam, momentum analysis, and lead plate chambers were then recorded on 35 mm film. Sets of these pictures were taken with the magnet in both polarities and with the target in place and the target removed.

C. Visual Selection of Events

The film of these events constituted the raw data and was first scanned visually in a search for what were considered to be $K^o \rightarrow \pi^+\pi^-$ decays. The visual requirement was that there be two tracks curving in opposite directions in the top view and that the two tracks appear to arise from the same physical location in both the top and side views. In general, this meant that each supposed pion traveled through at least three momentum analysis chambers in order to ascertain its direction of curvature. The efficiency for visually discovering these candidates is given in the following table:

TRIGGER	TARGET	POLARITY	EFFICIENCY			
			SCANNER I	SCANNER II	SCANNER III	TOTAL
K^o	Empty	A	98.1%	98.5%	____	99.2%
		B	96.0%	92.9%	90.6%	98.6% *
K^o	Pt	A	97.0%	99.2%	____	99 %
		B	98.5%	97.1%	97.8%	99.3%
K^+	Pt	A	98.0%	____	____	98.0%
		B	99 %	99 %	____	99 %

* Poor quality pictures resulted in anomously low scanning efficiency.

D. Measurement of Events

Next, measurements were made of the spark images of the
film of these candidates using Hydel encoding machines. There were
simple geometric and administrative requirements placed upon the
events through computer analysis and these are listed in Appendix
B. The events were remeasured and corrected if they failed these
requirements.

E. Kinematic Analysis of Events

After this initial screening, the candidates were analyzed
kinematically by computer. First, the encoded data were put through
a computer program for the reconstruction of the spark images'
coordinates to their actual physical locations in the apparatus
and then each set of supposed pion spark tracks was fit to helices.

From the parameters of these helices and the beam spark
locations, a kinematic analysis was made that charged particles
in the momentum analysis chambers were pions and all the kinematic
quantities of dipion system were calculated. The most important of
these is the dipion mass, which, for example, with a K^o trigger has
a majority of the candidates with a dipion mass within 20 MeV/c^2
of 497.7 MeV/c^2, the K^o mass. If the spark formation, measuring,
and computing resolution were perfect, we would expect nearly all
of these events to be within one MeV/c^2. The shape and width of the
dipion mass distribution is consistent with the measured spark

jitter and measuring accuracy. This brings up the question, what about the other events? Where did they come from?

F. Backgrounds

One source of events would be other neutral particles or other decay modes of the K^o. Most neutral particles decay very near to their production point for the momenta observed. The only known ones that do not are γ, ν, n, Λ, and Ξ^o. The last two cannot be directly produced by an incident K^+ because of strangeness conservation and 3.0 GeV/c is well below pair production threshold for these particles. The neutron has a long lifetime, so that one would not expect a significant number of decays inside the apparatus. On the other hand, any of the particles mentioned could interact with the matter in the apparatus and produce charge particle pairs. The neutrino has such a low interaction probability that we can rule it out as a source of charged pairs; however, a γ is likely to produce electron pairs by conversion in the aluminum foil of the momentum analysis chambers, etc. This process is such that roughly one γ in a hundred from the target is expected to convert. The neutron is much less likely to produce a charged pair. The K^o, in addition to its decay mode, has a $\pi^o \pi^o$ decay mode, which can also give rise to electron pairs either by Dalitz decay (approximately one pair for every 85 $K^o \rightarrow \pi^+\pi^-$) or by conversion of the γ's from the π^o's. The other decay modes of the K^o have rates so slow as to be a small part of the background.

Another source of this background could be random coincidence of two stray particles of opposite signs. These would appear off to the side of the chambers or at the beginning of the momentum analysis chamber array, because the efficiency of the spark chambers was better than 90%; thus, crossing tracks would be observed and not accepted.

Another possible source of the events would be actual $K^o \to \pi^+\pi^-$ decays in which one or both pions had undergone some interaction. Only about one in two thousand kaons is expected to have a pion either interact in the momentum analysis spark chambers or decay.

With these things in mind, the following empirical study was made on the set of data taken with the platinum target removed under a K^o trigger. After kinematic analysis, the events were separated into three classes.

CLASS	REQUIREMENT	POPULATION	% OF TOTAL
I.	$480 \leq m_{\pi\pi} \leq 520$ MeV/c^2 $m_{ee} \geq 200$ MeV/c^2	408	67.8%
II.	$m_{ee} \leq 200$ MeV/c^2	118	19.6%
III.	OTHERS	76	12.6%

The thought was that Class I would be $K^o \to \pi^+\pi^-$ with great likelihood; Class II would be electron pairs; and Class III would be stray tracks, etc. Next, every event in Classes II and III was rescanned, with the results of the kinematical analysis in hand.

The result of this scan for Class II was that 83%, i.e. 98 events, were obviously pairs, either from the showers in the lead plate chamber or their topology. Eighty-seven of these (90% had been designated as pairs or probable pairs during the initial scan for $K^o \rightarrow \pi^+\pi^-$ when there had been no emphasis on looking out for pairs. Twelve events (10.2% of Class II) were thought to be $K^o \rightarrow \pi^+\pi^-$ in which one pion had a high momentum and one pion had a low momentum, the kinematics of which would normally result in a pair mass below 200 MeV/c^2. These events were added to Class I. Six events (5.1% of Class II) were not clearly anything and were placed in Class III. Two events were clearly stray tracks, as one particle had the direction and location of the beam and a momentum of $\sim$ 3 GeV/c. These events were also added to Class III.

After this it appears that Class II consists entirely of events that are electron pairs. No events have an electron pair mass greater than 100 MeV/c even though the mass was allowed to take on values up to 200 MeV/c. Also, the di-electron mass spectrum compares well with the spectra from two other sources. The first source is a set of pairs selected to have both particles displaying good characteristic electron showers in the lead plate chamber. The second source was supplied by Dr. T. Romanoski of Argonne National Lab from what he thought were electron pairs from Dalitz decay of π^o's.

This would suggest that for every six $K^o \rightarrow \pi^+\pi^-$ observed, approximately one electron pair is seen. However, half of these pairs seem to come from upstream, mostly appearing to convert in

the foils of the side chambers and some significant fraction in the main beam chamber. Even so, only half the remaining would be expected to come eventually from $K^0 \to \pi^+\pi^-$; one might suppose the others to come from π^0, etc. produced in the target by the incident K^+. Next, Class III was processed and the result of the rescan was:

a) 25% were felt to be incorrectly measured

b) 20% were thought to be stray tracks

c) 55% were apparently good $K^0 \to \pi^+\pi^-$ events.

These were then remeasured and reprocessed.

The results of the remeasure and rescan of these Class III events were:

51% were thought to be $K^0 \to \pi^+\pi^-$.

27% were apparently stray tracks.

12% were apparently real Vees whose kinematics indicated that they were unlikely to be $K^0 \to \pi^+\pi^-$.

6% should not have been included in the sample (e.g., too few sparks, etc.)

4% were Vees which had a leg that had undergone an interaction or had some spark segments out of place.

For the most part, the events which were thought to be $K^0 \to \pi^+\pi^-$ were either very old and had many sparks missing or appeared in only a few spark chambers. These events could easily be moved into the appropriate mass range by small (on the order of spark jitter) displacements of their spark image locations.

This same type of classification and rescanning was done for the

data from the platinum target. This reworking of the data was not as intensive because there was less background. The result was that the K^o data appears to break down into the following:

94% $K^o \rightarrow \pi^+\pi^-$

3% $\gamma \rightarrow e^+e^-$

3% others.

V. Distributions and Spectra of the Data

The electron pairs and stray tracks were removed from the target full and target empty K^o trigger events. These events were then analyzed as pion pairs and later as $K_1^o \rightarrow \pi^+\pi^-$. The results of this analysis were utilized by a Monte Carlo program to calculate the detection efficiency for each event. Each event's momentum, angle to the incident K^+, and decay radius were held constant and a detection efficiency was determined for each event. Combining all these parameters, a plot was made of the proper time from production to decay versus frequency and corrected for efficiency. Both these spectra are fit very well by the published life time of the K_1^o, 0.862×10^{-10} seconds (i.e. $\pm 8\%$ of this value). The dipion mass spectrum was centered at 498 MeV/c^2 and had a half width at half height of ± 4 MeV/c^2.

The detection efficiency program was again run holding only the momentum and angle to the incident K^+ constant, varying the azimuthal angle, decay angles, and decay radius. From the other calculated parameters and detection efficiency, one has the following distributions:

(1) Momentum   (See Figures VII and VIII.)

(2) Angle   (See Figures IX and X.)

(3) $\dfrac{d\sigma}{dt}$ (See Figures XI and XII.)

as measured in the laboratory for Pt and scintillation targets

with a downstream veto.

The following $K^o \to \pi^+\pi^-$ production rates were measured for these configurations:

TRIGGER	TARGET	PRODUCTION RATE $K^o \to \pi^+\pi^-$	EFFECTIVE CROSS-SECTION FOR K^o PRODUCTION
K^+	Pt	$2.7 \times 10^{-3} \pm 10\%$	65.0 mb (for platinum)
K^o	Pt	$0.64 \times 10^{-3} \pm 3\%$	15.5 mb
K^o	Scintillator	$0.022 \times 10^{-3} \pm 5\%$	3.0 mb

VI. Theoretical Model

The following model of K^+ charge exchange (and other reactions) on platinum was suggested by Professor R. J. Glauber of Harvard University. It is based on the following assumption. First, the incident K^+ is attenuated as it passes through the platinum nucleus according to its free total cross-section, σ_T.

$$I(T) = I_0 \; e^{-\sigma_T T}$$

where I_0 is the original intensity of the K^+ beam and I is the intensity of the K^+ beam after traversing a nuclear thickness of matter T, i.e. $T = \int \rho(\vec{l})d\vec{l}$ where $\vec{l}$ is the path of the K^+ and ρ is the nuclear density along this path. This assumes random distribution of nucleons, specifically no clusters of nucleons. If there are clusters, this has the effect of decreasing the attenuation; if the K^+ misses one nucleon it tends to miss all the nucleons in the cluster[2]. This also assumes that one can use an average proton-neutron total cross-section over the whole nucleus. For 3 GeV/c the K^+N isotopic spin zero and one total cross-sections are estimated to be the same to 6%[3].

The second assumption is that the nucleon undergoing reaction can be treated as a free particle with same momentum. For high energy K^+ with momentum on the order of 3 GeV/c and with a binding energy of the nucleons on the order of 10 MeV, the binding of the nucleon has an effect only at small momentum transfers[4]. There is, however, a larger effect arising from the fact that the

nucleons are fermions and must obey the Pauli exclusion principle. This will be discussed below.

An example of the simplest charge exchange process follows.

(1)
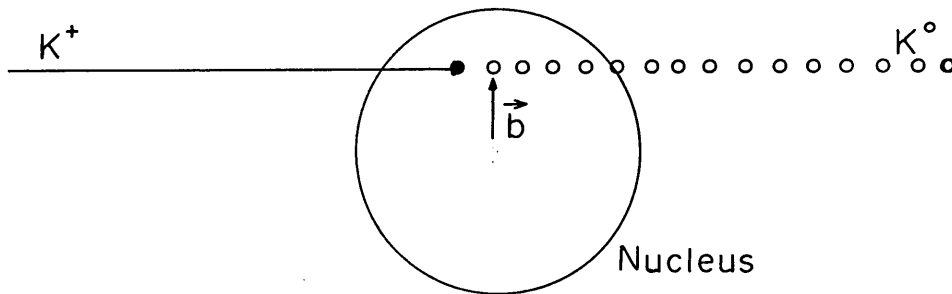
The cross-section for this reaction would be given by

$$\frac{d\sigma}{dq}(1) = \frac{d\sigma}{dq} \times \frac{1}{\sigma} \int e^{-\sigma_T T_+(b)} \int_0 dT(\vec{b}) \ dT(\vec{b}) \ e^{-\sigma_T T_0(b)} \ d^2b$$

Attenuation	Probability	Attenuation
of K^+ beam	of Interaction between T and T + dT	of K^o beam

$$\times \left\{ 1 - S(\vec{q}) \right\}$$

suppression factor because
of Pauli exclusion principle

where

σ = cross-section for $K^+ n \to K^o p$

$\frac{d\sigma}{dq}$ = differential cross-section for $K^+ n \to K^o p$

σ_T = total cross-section for KN

$T(\vec{b}) = \int_{-\infty}^{+\infty} \rho(\vec{b} + \hat{k}z) \ dz$ = nuclear thickness

$\vec{b}$ is the impact parameter.

ρ is nuclear density function and the approximation is
made that the scattering angle is zero as far as the amount of
nuclear material encountered is concerned.

$\int\limits_{f}$ is fraction of nucleons that are neutrons.

$\left[1 - S(\vec{q})\right]$ is suppression factor for Pauli exclusion.

The next least complicated form of K^+ charge exchange would
be double scattering as represented in the following diagrams:

(2)   (a)

(b)
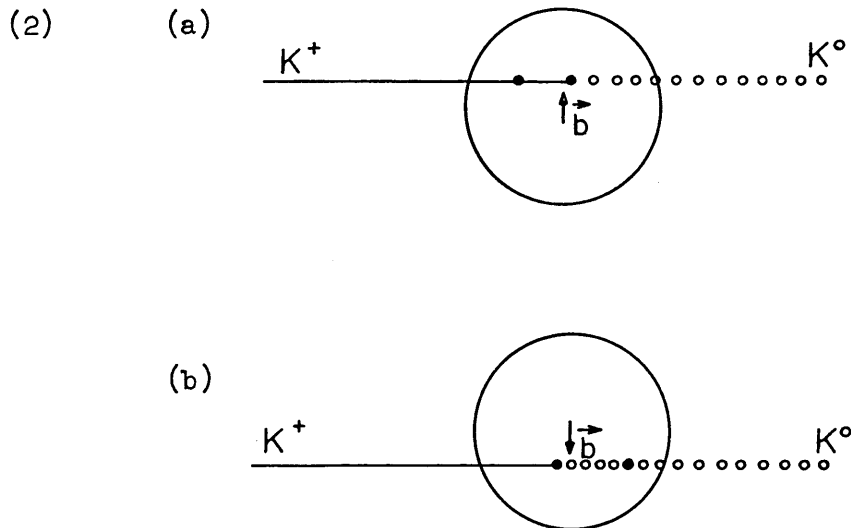
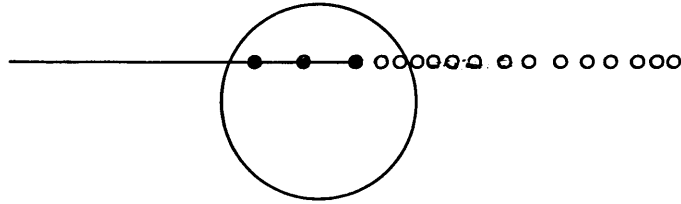In this case the expression for the cross-section would be

$$\frac{d\sigma}{d\vec{q}}(2) = \int_{-\infty}^{+\infty} d\vec{q_1} \int_{0}^{T+} e^{-\sigma_T T} + \frac{d\sigma_{el}}{d\vec{q}} dT_1 \int_{T_+}^{T_+ + T_1} e^{-\sigma T_1} + \frac{d\sigma_{ex}}{d(\vec{q}-\vec{q_1})} \int dT_2$$

$$x \quad e^{-\sigma_T T_2} d^2 b \quad x \quad \left(1 - S(\vec{q_1})\right)\left(1 - S(\vec{q} - \vec{q_1})\right)$$
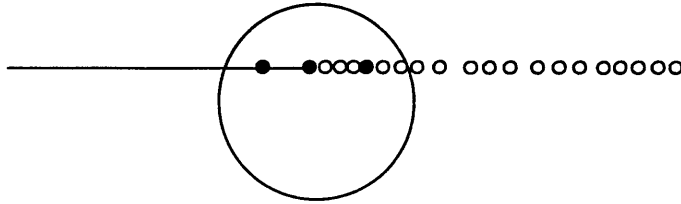
   + the conjugate expression.

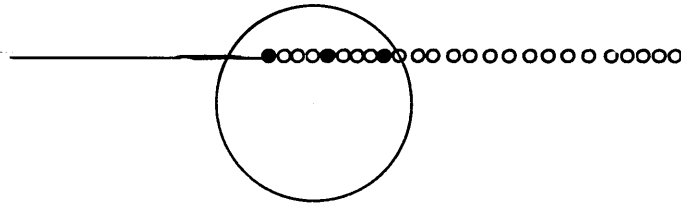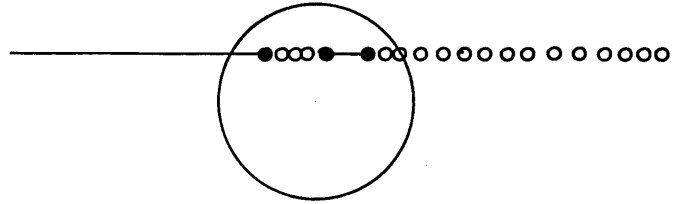Likewise there can be triple scattering, e.g.

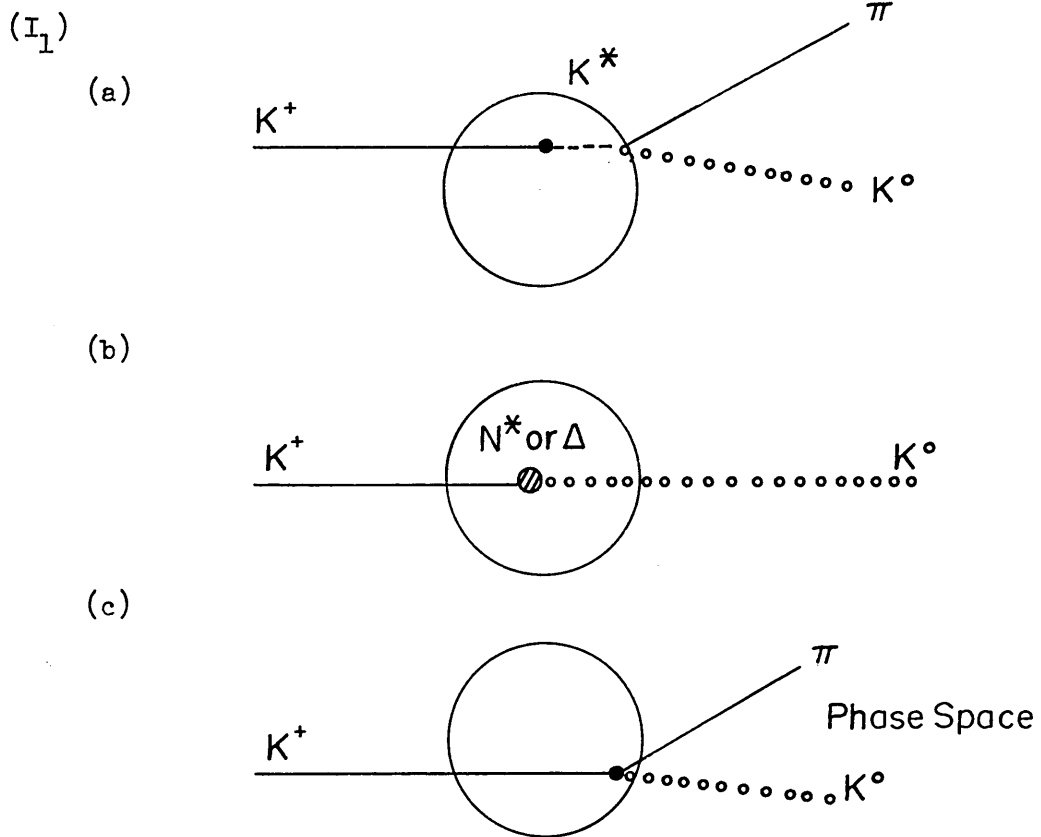(3)   (a)

(b)

(c)

(d)

$$\frac{d\sigma}{d\vec{q}}(3) = \int d^2b \int d\vec{q}_1 \, \frac{d\sigma}{d\vec{q}_1} \int d\vec{q}_2 \, \frac{d\sigma}{d\vec{q}_2} \, \frac{d\sigma}{d(\vec{q}-\vec{q}_1-\vec{q}_2)} \frac{1}{\sigma} \frac{1}{\sigma} \frac{1}{\sigma} \sigma dT_1 \sigma dT_2 \sigma dT_3$$

$$x \left(1 - s(\vec{q}_1)\right) \left(1 - s(\vec{q}_2)\right) \left(1 - s(\vec{q}-\vec{q}_1-\vec{q}_2)\right) x \quad e^{-\sigma T_1} e^{-\sigma T_2} e^{-\sigma T_3}$$

and so on to higher orders.

The processes above could be described as quasi-elastic charge exchange, then we could have inelastic charge exchange, e.g. one additional pion

(I_1)

    (a)

    (b)

    (c)

And of course these can have multiple scatterings. In addition, the two pion modes can occur

(II_1)
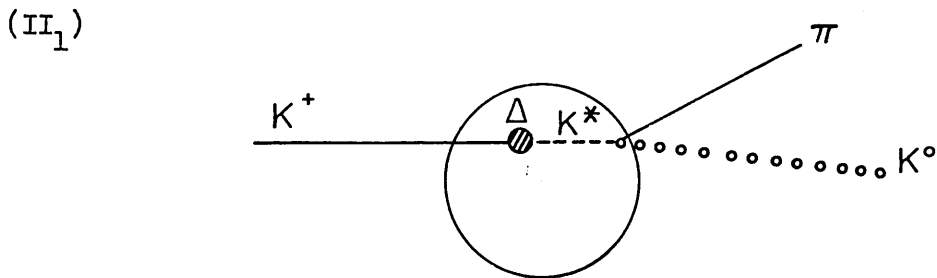
and so forth.

What does this tell us about the cross-sections in more detail? If the K^o and K^+ have the same total cross-section, the expressions for simple charge exchange become (without the Pauli suppression factors):

$$\frac{d\sigma}{d\vec{q}}(1) = \left\{ \int e^{-\sigma T(\vec{b})} T(\vec{b}) d^2b \right\} \times \frac{d\sigma_{ex}}{d\vec{q}}$$

$$\frac{d\sigma}{d\vec{q}}(2) = \left\{ \int e^{-\sigma_T T(\vec{b})} \frac{1}{2} \left(T(b) \right)^2 d^2b \right\} \times \int 2 \frac{d\sigma_{el}}{d\vec{q}'} \frac{d\sigma_{ex}}{d\vec{q} - \vec{q}'} d\vec{q}'$$

$$\frac{d\sigma}{d\vec{q}}(3) = \left\{ \int e^{-\sigma_T T(\vec{b})} \frac{1}{6} \left(T(\vec{b}) \right)^2 d^2b \right\} \times$$

$$\iint \left(3 * \frac{d\sigma_{el}}{d\vec{q}'} \frac{d\sigma_{el}}{d\vec{q}''} \frac{d\sigma_{ex}}{d\vec{q}-\vec{q}'-\vec{q}''} + \frac{d\sigma_{ex}}{d\vec{q}'} \frac{d\sigma_{ex}}{d\vec{q}''} \frac{d\sigma_{ex}}{d\vec{q}-\vec{q}'-\vec{q}''} \right) d\vec{q}' d\vec{q}''$$

A good approximation for $\frac{d\sigma_{el}}{dq}$, the differential cross-section foe elastic scattering, is

$$\frac{d\sigma_{el}}{dq} = A_{el} \, e^{-Kq^2}$$

where A_{el} and K are constants. This formulation is good out to high momentum transfers where much less than 1% of the events occur. This form is also a good approximation for the charge exchange differential cross-section between 0.25 $(GeV/c)^2$ and high momentum transfers. If these shapes held, one would have

$$\frac{d\sigma}{d\vec{q}}(1) = A_1 \, e^{-Kq^2}$$

$$\frac{d\sigma}{d\vec{q}}(2) = A_2 \, e^{-Kq^2/2}$$

$$\frac{d\sigma}{d\vec{q}}(3) = A_3 \, e^{-Kq^2/3}$$

This reflects the fact that each scattering tends to have the lowest momentum transfer possible for a given total momentum transfer. For example, the main contributions from double scattering at momentum transfer q comes from the region of 1/2 q for reactions with the same coefficient K. Thus, for instance, the shape of $\frac{d\sigma}{dq}(2)$ in the region $q^2 = -1.0$ $(GeV/c)^2$ is determined by the elastic scattering and charge exchange differential cross-sections at $q^2 = -0.25$ $(GeV/c)^2$, i.e. the interval -0.1 to -0.6 $(GeV/c)^2$. For this value of q^2 and higher four momentum transfer, one would expect $\frac{d\sigma}{dq}(2)$ to go as $e^{-Kq^2/2}$.

When one puts in the Pauli exclusion suppression factor, a bite is taken out of the leading edge of $\frac{d\sigma}{dq}(1)$ according to the momentum distribution of the nucleus in platinum. The magnitude of this bite is calculated to be $q^2 = 0.02$ $(GeV/c)^2$ with a principle spread of the same value. However, the shapes of $\frac{d\sigma}{dq}(2)$, $\frac{d\sigma}{dq}(3)$, etc. are not changed to first order as multiple scatterings of larger momentum transfers cancel themselves into this region of small momentum transfer.

The other differential cross-sections can also be approximated in the same form; however, these are not quite as accurate as for elastic scattering. The combined cross-sections, i.e. if for processes α and β

$$\frac{d\sigma}{dq}\alpha = A_\alpha \, e^{-K_\alpha q^2}$$

$$\frac{d\sigma}{dq}\beta = A_\beta \, e^{-K_\beta q^2}$$

then the differential cross-section for the following
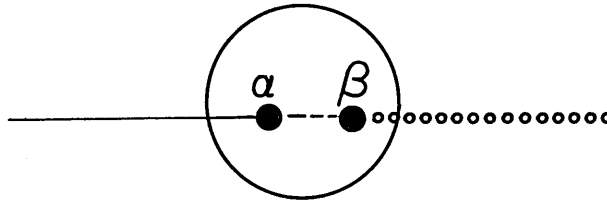
would be

$$\frac{d\sigma}{dq}\alpha\beta = A_{\alpha\beta} \, e^{-\frac{K_\alpha K_\beta}{K_\alpha + K_\beta} q^2}$$

For a total momentum transfer of q, process α tends to contribute events from the region of momentum transfer

$$q_\alpha = q \times \left[\frac{K_\beta - K_\alpha K_\beta}{K_\beta - K_\alpha} \right]$$

and likewise from β,

$$q_\beta = q \times \left[\frac{K_\alpha - K_\alpha K_\beta}{K_\beta - K_\alpha} \right].$$

The next subject to discuss is the suppression factors created by the exclusion principle. In order to calculate them one must know the nucleon momentum distribution and then he can apply the exclusion principle. If one assumes that the nucleus is a degenerate Fermi gas, then the nucleons occupy all the states up to 21 MeV of

kinetic energy[5]. Another source of this distribution is to see what has been measured. The nuclear momentum spectra have been observed for Be and C and fitted with gaussian distributions whose 1/e points are at 20 and 19.3 MeV respectively[6,7].

With this in mind, 20 MeV was chosen as the potential well depth in which the nucleons are assumed to reside. (A study was done with a 100 MeV well depth and this value was found to be consistent with the data; on the other hand, it would have been reasonable to use a 30 MeV well depth, but 20 MeV seemed to be a better choice because it gives an average binding energy of 8 MeV per nucleon[8,9].

For a first try, the nucleons were assumed to have the momentum distribution of a degenerate Fermi gas located within the nucleus. When there is an interaction in which a nucleon is scattered (its charge may or may not be changed) there must be enough momentum transferred to raise the resulting nucleon to a momentum state which is not occupied by other nucleons in the recoiling nucleus. Thus

$$S(\vec{q}) = \Theta\left(P_F^2 - \left[(\vec{q} + \vec{P}_N) - \vec{P}_N/A\right]^2\right)$$

where

$$\Theta(x) = \begin{cases} 0 & x < 0 \\ 1 & x \geq 0 \end{cases},$$

P_F is the momentum of highest occupied state, $\vec{P}_N$ is the momentum of the struck nucleon, A is the number of nucleons in the recoiling nucleus, and $\vec{q} + \vec{P}_N$ is the three-momentum of the resulting outgoing nucleon . For platinum this requires that the three-momentum transferred be such that the magnitude of $\vec{q} + \vec{P}_N$ is

greater than $P_F = 195$ MeV/c ± 1 MeV/c (error being from the whole nuclear motion)[10].

For a gaussian distribution of momentum, i.e.

$$P(\vec{p})d\vec{p} = e^{-P^2/P_0^2}\ d\vec{p}$$

this corresponds to a spatial distribution

$$\rho(\vec{r})\ d\vec{r} = \frac{1}{\pi^{3/2}R_0^3}\ e^{-r^2/R_0^2}\ d\vec{r}$$

per nucleon. The number of states is then

$$N(\vec{p})d\vec{p} = 1\ d\vec{p}$$

thus, the number of states unoccupied is

$$\left[1 - e^{-P^2/P_0^2}\right]\ d\vec{p}$$

In general, if one takes the case where the nucleons are distributed in the nucleus according to a spatial density function $\rho(\vec{r})$ normalized so that

$$\int\rho(\vec{r})\ d\vec{r} = 1$$

then

$$S(\vec{q}) = \int e^{i\vec{q}\cdot\vec{r}}\ \rho(\vec{r})\ d\vec{r}. \qquad [11]$$

Since the number of momentum states available for nucleons of each kind and spin state is

$$N\ d\vec{p} = \left(\int\rho(\vec{r})\ d\vec{r}\right) d\vec{p} = 1\cdot d\vec{p}$$

and since the momentum spectrum goes as $S(\vec{q})d\vec{q}$, the number of unoccupied states is

$$\left[1 - S(\vec{q})\right]\ d\vec{q},$$

there is the additional possibility of coherent scattering of the

incoming or outgoing particle by the nucleus. The differential
cross-section for coherent scattering is

$$\frac{d\sigma}{dq} \text{ coherent} = A^2 \left| f(\vec{q}) \right|^2 S^2(\vec{q}) \ .$$

Because of the internal momentum spectrum of the nucleus, coherent
scattering is strongly peaked in the forward direction and limited
to small angles. For example, consider the gaussian momentum
distribution; the form factor $S(\vec{p})^2 = e^{-2p^2/p_0^2}$ is down to $1/e$
at an angle of 0.05 radians (2.7 degrees). This is the angle at
which the degenerate Fermi gas model cuts off entirely and is the
same size as the experimental resolution. Because of this, coherent
scattering has been ignored.

Calculations were done with several different $S(\vec{q})$'s. A change
in $S(\vec{q})$ has a predictable impact. In most cases, the effect is small
because the effect is the same size as the experimental resolution.
Two quantities that are more sensitive than most are the four-
momentum transfer and the K^o laboratory momentum spectra for
$K^+ + n \rightarrow K^o + p$ events. For the four-momentum transfer, there is
a removal of events in the region $t = 0.0$ to 0.15 $(GeV/c)^2$ with
three quarters of the events depleted between 0.0 and 0.07 $(GeV/c)^2$.
The difference between the gaussian and degenerate Fermi gas cases
was negligible for two thousand events. As for the momentum
spectrum, since there is a minimum momentum transfer and energy is
conserved, some momentum from the incident K^+ must be given to the
outgoing nucleon. This means that the outgoing K^o has a momentum
spectrum whose upper bound is set by physics of the charge exchange

process, namely the four-momentum transfer spectrum. The only data available on $K^+ + n \rightarrow K^o + p$ has been taken on neutrons bound in nuclei so that their measured four-momentum transfer distribution is going to have been affected by the exclusion principle. This effect has been corrected for in estimating this differential cross-section.[12] The gaussian and degenerate Fermi gas models appear to take nearly the same bite out of the highest momentum K^o's. The effect was to cut out about half of the highest-lying third of the events.

In order to calculate these cross-sections for platinum, one need only know the cross-sections for the various reactions with free nucleons.

Cross-Sections

Most of the various cross-sections have only been measured for K^+ on protons[2, 12, 13]; however, one can use charge independence, etc., to estimate the rest of the cross-sections. These estimates are:

$$\sigma_{KN} \text{ Total} = 18.0 \text{ mb}$$

$$\sigma_{KN} \text{ Elastic} = 5.0$$

$$\sigma \ K^+ + n \rightarrow K^o + p = 0.75$$

$$\sigma \ KN \rightarrow K^o + \Delta \ (1236) = 0.7$$

$$\sigma \ KN \rightarrow K^*N = = 1.5$$

$K^{*o} \rightarrow K^o \pi^o$ 1/3 of the time; $K^{*+} \rightarrow K^o \pi^+$ 2/3 of the time.)

$$\sigma \; KN \to \overset{o}{K} N\pi \qquad \cong \qquad 0.7$$

$$\sigma \; KN \to \overset{*}{K} \Delta \, (1236) \qquad \cong \qquad 0.7$$

and so on.

Further, $\overset{o}{K} \to \pi^+\pi^-$ is 34.5% of all the $\overset{o}{K}$ decay modes.

We can use this to make predictions for the various sets of data. For this calculation we will assume that the nucleus is spherically symmetric. The first set of data to be considered is the target empty with the downstream veto counter in use, i.e. $\overset{o}{K}$ target empty.

$K^+ + N \to$	$\overset{o}{K}_1 \to \pi^+\pi^-$ DETECTION EFFICIENCY	FRACTION WITH NO CHARGED PION IN FINAL STATE	RELATIVE NUMBER OF SOURCES
$\overset{o}{K} p$	0.78	1	1.0
$\overset{o}{K} \Delta^+ (1236)$	0.75	2/3	1.0
$\overset{o}{K} \Delta^{++} (1236)$	0.75	0	1.44
$\overset{o \, *}{K} p$	0.56	1/3	1.0
$\overset{o \, *+}{K} p$	0.56	0	1.44
$\overset{o}{K} \overset{o}{\pi} p$	0.58	1	1.0
$\overset{o}{K} \pi + n$	0.58	0	1.0
$\overset{o}{K} \pi^+ p$	0.58	0	1.44
$\overset{o \, *}{K} \Delta^+ \to \overset{o}{K} \overset{o}{\pi} \Delta^+$	0.45	2/3	1.0

If we say that for the $\overset{*}{K}$ reactions the charged pions always run the veto while for the $\overset{o}{K} \Delta \,(1236)$ events ninety percent do, and for $\overset{o}{K} \pi^+ n$ three quarters of the events do, we have

	EFFECTIVE CROSS-SECTION	EXPECTED FRACTION OF DATA
$K^o p$	0.58	33%
$K^o \Delta^+$ (1236)	0.35	20%
$K^{o*} p$	0.28	16%
$K^o \pi^o p$ $K^o \pi^+ n$	0.35	20%
$K^{o*} \Delta^+ \rightarrow K^o \pi^o \Delta^+$	0.2	11%

$$1.76$$

The predicted rate of K^o production is then 0.034×10^{-3} K^o per incident K^+. The measured value is 0.022×10^{-3} K^o/K^+. The root of the difference would seem to be the protons which have enough momentum to reach the veto scintillation counter and veto the event. This is quite different from the case when the platinum target is in place, because of the extra stopping power of the platinum and its extra factor of ten in total target thickness. There is also the added factor of secondary reaction by the outgoing baryon within the same nucleus. This would say that 1/3 of all protons produced escape to the veto counter.

Now one can take a closer look at the constituent classes of these events. The reactions $K^+ + n \rightarrow K^{o*} + p \rightarrow K^o \pi^o p$ and $K^+ + n \rightarrow K^{o*} \Delta \rightarrow K^o \pi^o \Delta$ are expected to be $\sim 30\%$ of the data; the latter reaction will be suppressed more because escaping protons have a higher momentum spectrum than the others. Because the

pi-zero is carried forward with the K^o, one would expect to see the
γ-rays from the π^o decay converting in the lead chamber. About
one sixth of the time, one should see both gamma rays; one-half
the time either of them; and one-third, neither. Thus, about 18%
of the events should have γ-rays present in them from K^{o*} events.
The actual number observed is about 17%, some small fraction of
which must be from $K^o \Delta^+ \to K^o \pi^o p$ and $K^o N^{*+} \to K^o \pi^o p$ (the solid
angle is $\sim 1/10$ but with relativistic folding is less, since Δ's
come out at angles slightly greater than 45°.) A plot of the K^o
momentum spectrum for the events with extra γ-rays present shows the
flat shape exhibited by the $K^{o*} p$ and $K^{o*} \Delta^+$ as calculated by the
Monte Carlo programs and not the peaked shape of the bulk of the
data or the $K^o \Delta$ Monte Carlo events.

The reaction $K^+ + n \to K^o + p$ is predicted to produce 30% of
the events observed. A check of this was made by plotting a two-
dimensional histogram of parallel and perpendicular incident K^+
components of the K^o's momentum. On this plot, one finds a band
of events corresponding to the Monte Carlo $K^+ + n \to K^o p$ charge
exchange events; these events comprise 37% of the data. This prob-
ably reflects a higher attrition rate for other events due to
escaping charged particles (protons and pions). The rest of the
data could come from either $K^o \pi N$ phase space or KN^* and $K\Delta$ or both.
There seems to be no easy way to sort them out as their spectra are
similar.

The momentum distributions calculated by the Monte Carlo
programs for the outgoing baryons produced in the kaon-nucleon

interactions have the following properties. This is the momentum as calculated for the baryon _in situ_ the nucleus. For events produced in the scintillator:

(1) 75% of all protons from $K^+ + n \rightarrow K^o + p$ are initially at wide enough angles to miss the veto counter.

(2) 95% of all the Δ^+ from $K^+ + n \rightarrow K^o + \Delta^+$ are initially at angles that will intercept the veto counter.

(3) 50% of the protons from $K^+ + n \rightarrow K^o + p$ are initially at angles to miss the veto counter.

(4) 95% of all N^*'s from $K^+ + n \rightarrow K^o + N^*$ are initially at angles where they will intercept the veto counter.

There is the question of what happens to their momentum as these baryons, some of which decay, leave the nucleus. Presumably they are slowed down along their direction of travel by 200 MeV/c for nucleons and some similar amount for pions. (We glossed over this for the K^+, K^o and K^* by assuming the K^o or K^* were slowed down by the same amount as the K^+ was sped up, i.e. by saying kaons did not know the nucleus was there except to interact with individual nucleons.)

Another set of data is that in which the platinum was in place and the only trigger requirement was that a K^+ entered the target. The total cross-section for $K^+ + p \rightarrow K^o +$ anything is approximately 6.3 mb. The geometric detection efficiency goes down dramatically with increasing number of pions produced, first because the K^o has a lower momentum and secondly because it will tend to come out at wider angles.

If we take reasonable averages of geometric efficiencies for the various ways these pion modes occur, we have the following estimates:

REACTION PRODUCT	GEOMETRIC EFFICIENCY	CROSS-SECTION
K^o + p	0.85	0.75 (neutrons only)
K^o Nπ	0.66	2.3
K^o N$\pi\pi$	0.50	2.8
K^o N$\pi\pi\pi$	0.20	0.5

This is an effective cross-section of 3.0 mb for protons and 3.7 mb for neutrons. There is an additional factor of 42% to include double scattering events, and then another factor of 0.92 for the suppression due to the Pauli exclusion of fermions for those evetns with a neutron or proton as direct reaction products. Then there is the addition of 11% more material due to the two scintillators on both sides; all this has the effect of raising the effective cross-section per nucleon approximately 40% and predicting a production rate of 3.1 x 10^{-3} K^o per K^+. The rate measured was 2.7 ± 0.3 x 10^{-3} K^o per K^+.

The largest set of data we have to be treated by this model is the K^o target full data with the veto counter behind the target in use. Of all the reactions available for the K^+ triggered data, all but the following have charge particles that will nearly always enter the veto counter:

PRODUCT	σ mb	x	K^o EFFICIENCY
$K^o p$	0.75		0.85
$K^o \Delta^+$ (1236)	0.5		0.83
$K^o \Delta^{++}$ (1236)	0.75	(x 0.2 because of π^+ vetoing the event)	0.83
$K^{*o} p \to K^o \pi^o p$	0.5	(x 1/8 because of γ ray conversion in the platinum)	0.66
$K^o (N\pi)^+$	0.7		0.68
$K^o (\pi\pi N)^+$	2.8	(x 0.05 because of pions vetoing the event)	0.57

TOTAL   1.78

Each of these can have the outgoing K^o (or K^{o*}) scatter "elastically" on another nucleon. This happens about 0.4 as often as a single interaction takes place. There is, in addition, a suppression of these events due to the Pauli exclusion principle, etc. leading to a prediction of an effective cross-section of 25.6 mb, a rate of $0.85 \times 10^{-3} K^o/K^+$. The measured rate is $0.64 \times 10^{-3} K^o/K^+$.

The source of this discrepancy once again is probably the protons and pions escaping from the nucleus and entering the veto counter. The veto counter subtends a larger solid angle for the platinum target than for the scintillator, S_6. The events which are least affected through the mechanism of escaping protons and pions are the simple charge exchange type as the protons are already at wide angles and low momenta. The platinum target is effective in stopping these protons.

The second least affected events are $K^+ + n \rightarrow K^o + \Delta$ (1236) in comparison with the $K^o (N\pi)^+$ events. The protons come out at angles and momenta intermediate to the simple charge exchange events and the $K^o (N\pi)^+$ events.

In order to estimate this effect, one can assume that each outgoing baryon is slowed down by 200 MeV/c and that the platinum stops a 400 MeV/c proton on the average. By making this subtraction and range cut almost no simple charge exchange events are vetoed, about 20% of the $K\Delta$ events are vetoed and 50% of the $KN\pi$ events are vetoed.

One can use the estimated fraction of these various components to predict the K^o momentum spectrum as measured in the laboratory. Figure XIII shows the Monte Carlo calculated momentum spectra for $K^+ + n \rightarrow K^o + p$ and the same process with double scattering. Figure XIV shows the Monte Carlo calculation momentum spectrum for $K^+ + n \rightarrow K + \Delta$ (1236) and the same process with double scattering. Similar curves are produced for N^*'s and they are appropriately shifted down. A smoothed version represents $KN\pi$ phase space. As mentioned before, the momentum spectrum of $K^* p$ is flat and basically similar to $KN\pi$ phase space. See Figure XV for these curves. If we add these components together, we get the results shown in Figures XVI and XVII, depending upon the fractions that are mixed. The first figure has the $K^o p$ and $K^o \Delta$ events in the same proportion they would be if escaping protons had no effect on the veto, whereas the second figure has the $K^o \Delta$ events

suppressed by 25%. In both figures the other constituents have been

suppressed by the amount estimated to be caused by pions and protons

vetoing.

One may also observe the missing mass spectrum for this data.

The missing mass is calculated by assuming the incident K^+ struck

a free neutron at rest and then using the measured parameters of the

K^o to compute the mass of what is assumed to be the other outgoing

particle, i.e. the missing proton. See Figures XVIII and XIX for

the missing mass spectra for the platinum target and target

empty data. Figures XX and XXI are the Monte Carlo calculated

spectra for $K^o p$ and $K^o \Delta$. It is clear that there are considerably

more events with missing mass near 1200 MeV/c^2 in the platinum data

than in the target empty data, as expected. Likewise the high

mass tail on the target empty is flatter than that for the target

full. This is what one would expect from a heavy fraction of $K^* p$

events in comparison with the $K N \pi$ events. In general the outline

differences between these two spectra can be gleaned from knowledge

of the difference in the targets and target configurations and from

knowledge of the various reaction channels operating.

The differential cross-section $\frac{d\sigma}{dt}$, for platinum follows the

predicted double scattering cross-section from -0.7 (GeV/c)^2 out

to -1.5 (GeV/c)^2 where there is a lack of events for comparison.

However, the double scattering should only account for about 60%

of the events in this region; many of the reactions (e.g. $K^+ + n \rightarrow$

$K^o + \Delta$) have a tail on their differnetial cross-section which

extends into this region and contributes the remaining events. The differential cross-section for the target empty, primarily carbon and hydrogen nuclei, has a considerably steeper slope than that of platinum. Presumably this is due to three causes:

(1) There should be many fewer secondary scatterings in these nuclei than in platinum.

(2) There are fewer events of the $K^o \Delta$ type which contribute to this tail; on the other hand, there are more K^+ events which add to this tail, so these balance out.

(3) Because of less stopping power of pions and protons in the target empty case, large momentum transfer events probably have much lower efficiency than low momentum transfer events.

Nothing conclusive can be determined from this region of high momentum transfer due to the large effect of the detectors' efficiency in this region and because the differential cross-sections for many of these reactions are not well determined.

If one looks at the region of small momentum transfers, namely 0.0 to -0.03 $(GeV/c)^2$ there is also a definite difference between the platinum and target empty data. Relatively there are about twice as many events present in this region for the platinum target. One would expect this to occur as a result of double scattering. There sould also be a small contribution into this region due to coherent scattering also, but it is not significant.

Conclusions

The conclusion drawn from the comparison of these data and this model is that one can treat high energy kaon interactions with nuclei, specifically platinum, as independent kaon-nucleon interactions. The main modifications of a kaon-nucleon interaction from that of a free nucleon with a kaon arise from the momentum distribution of the nucleons in the nuclei. Namely, they are the density of final states available and the non-negligible momentum of the struck nucleus. One can observe this effect in the target empty data where the events though to be $K^+ + n \to K^o + p$ on carbon appear to stand out from the rest of the data. These events do not occur in the region corresponding to small momentum transfer and have a K^o vector momentum spectrum which is a band around the vector momentum locus one would expect for charge exchange from a free neutron. The width of this band corresponds very well to the Monte Carlo prediction for momentum distribution characterized by 20 MeV of kinetic energy (20 ± 15 MeV).

The platinum target data show this same lack of events for small momentum transfer in the band where the simple charge exchange events are expected. However, as opposed to the target empty, there is no clear gap between the $K^o p$ and $K^o \Delta$ bands but these regions are blurred together. This is just the region we expect the double scattered $K^o p$ events to be found and as predicted there are very few events for the target empty data and relatively many for the platinum target data.

Using this very simple model and measured cross-sections,

one should be able to estimate total cross-sections to as close as ten percent of their actual value depending upon how complicated the geometry is. One could certainly expect to estimate upper bounds for his cross-sections to this order of accuracy for various nuclei.

This analysis indicates that the basic kaon-nucleon interaction at high energies is not significantly altered by the presence of other nucleons to about the thirty percent level. The various reactions occur at the same rate and with the same differential distributions in the presence of the nucleus as for free nucleons to this level. To the resolution available here (± 100 MeV) there are no new reaction channels opened through simultaneous multiple excitement of the constituent nucleons. In other words, for high energy and momentum transfers with kaons, the nucleons in a nucleus are to first approximation free and uncoupled from each other. See Figures XVI and XVII.

FIGURES AND ILLUSTRATIONS

Figure I

Schematic drawing of apparatus

Includes:

(1)   Scintillation counters in beam telescope S_2, S_3, S_4, S_6, and V, the vetoing counter with hole in it, located downstream of S_4

(2)   Differential Čerenkov counter C

(3)   A lead collimator between counters S_2 and S_3

(4)   Three beam spark chambers

(5)   Eight momentum analysis spark chambers located inside Argo magnet
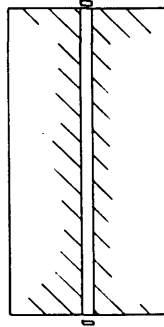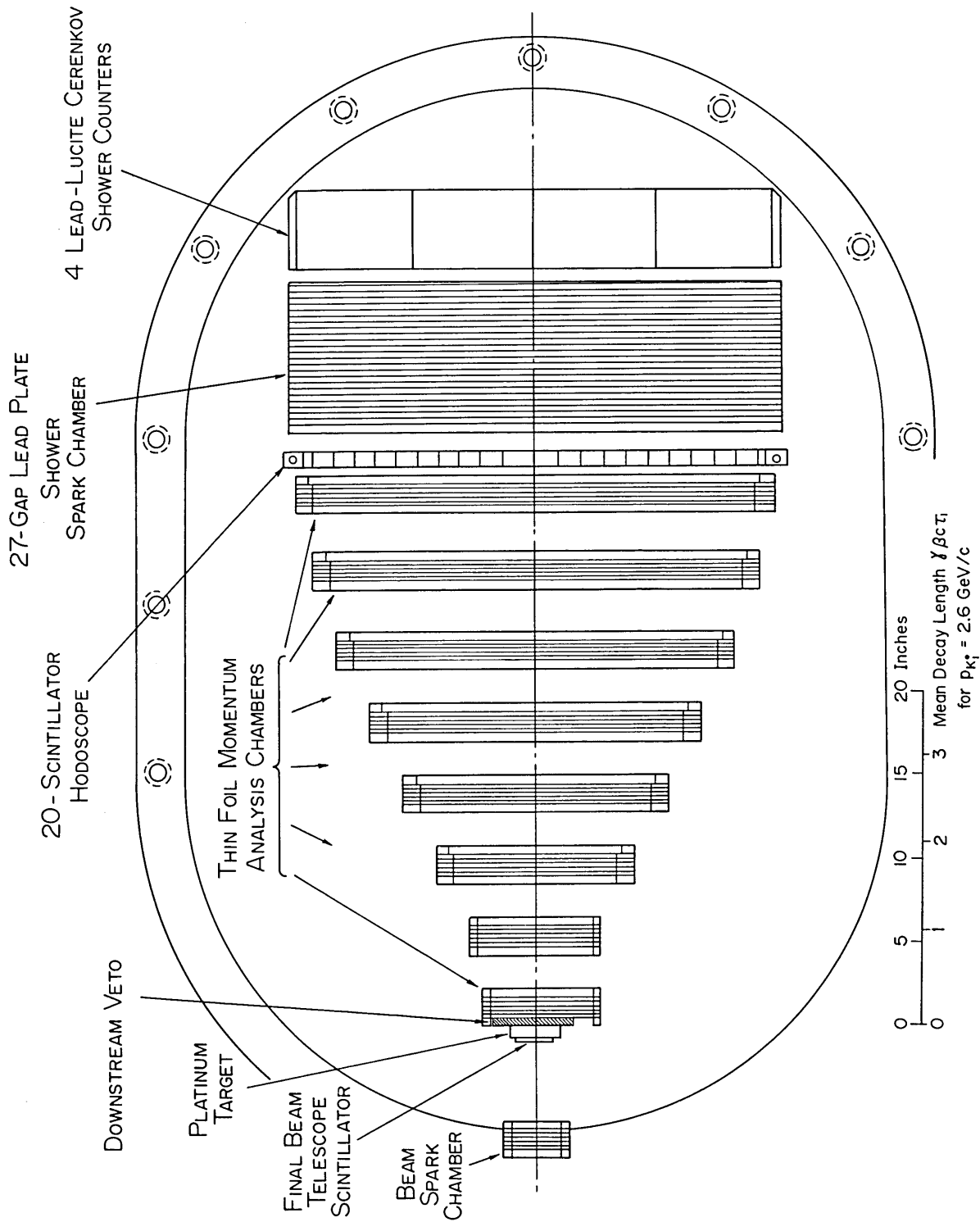
(6)   A multi-gap lead plate spark chamber

V

S_6

S_5

$\check{C}$

S_3

S_2

4 LEAD-LUCITE CERENKOV SHOWER COUNTERS

27-GAP LEAD PLATE SHOWER SPARK CHAMBER
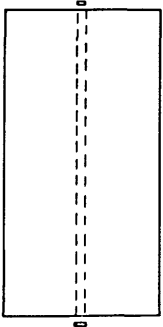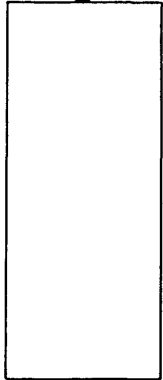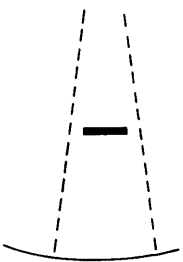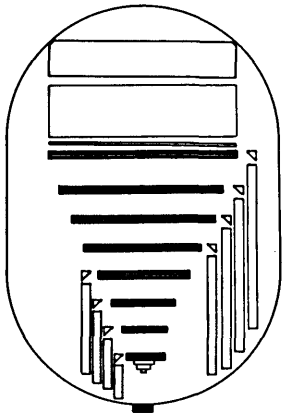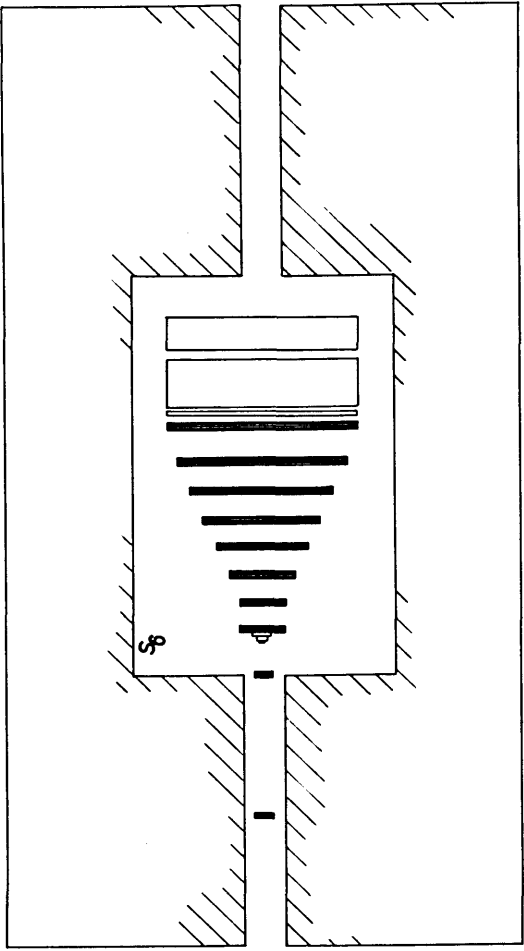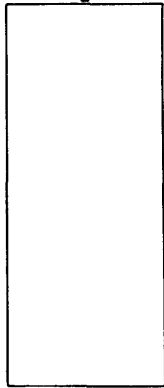
20-SCINTILLATOR HODOSCOPE

THIN FOIL MOMENTUM ANALYSIS CHAMBERS

DOWNSTREAM VETO

PLATINUM TARGET

FINAL BEAM TELESCOPE SCINTILLATOR

BEAM SPARK CHAMBER

20 Inches

Mean Decay Length $\gamma \beta c \tau_1$ for $p_{K_1^\bullet} = 2.6$ GeV/c

Figure II

Cerenkov counter pressure curves

The curve on the right was taken by Dr. T. Kycia in a special test at 85° F. The curve on the left is a composite of data taken on the counter as it was being used in the experiment.

with Separator on

π^+
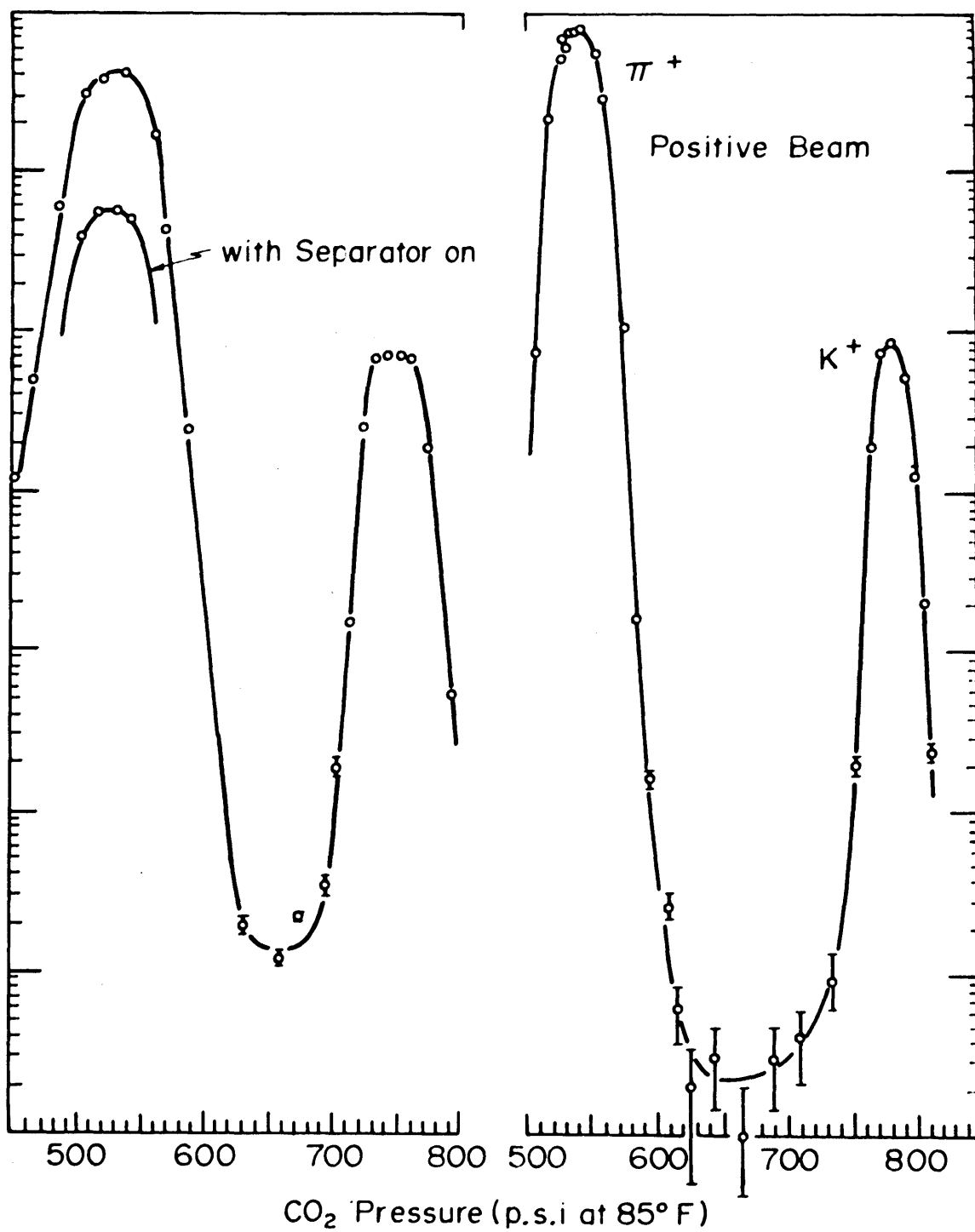
Positive Beam

K^+

CO$_2$ Pressure (p.s.i at 85° F)

Figure III

Beam entrance region magnetic field

A plot of magnetic field measurements was made by placing a Hall probe along the center line of the beam entrance region of Argo magnet. The solid curve represents the model of the magnetic field used in calculating beam trajectories.
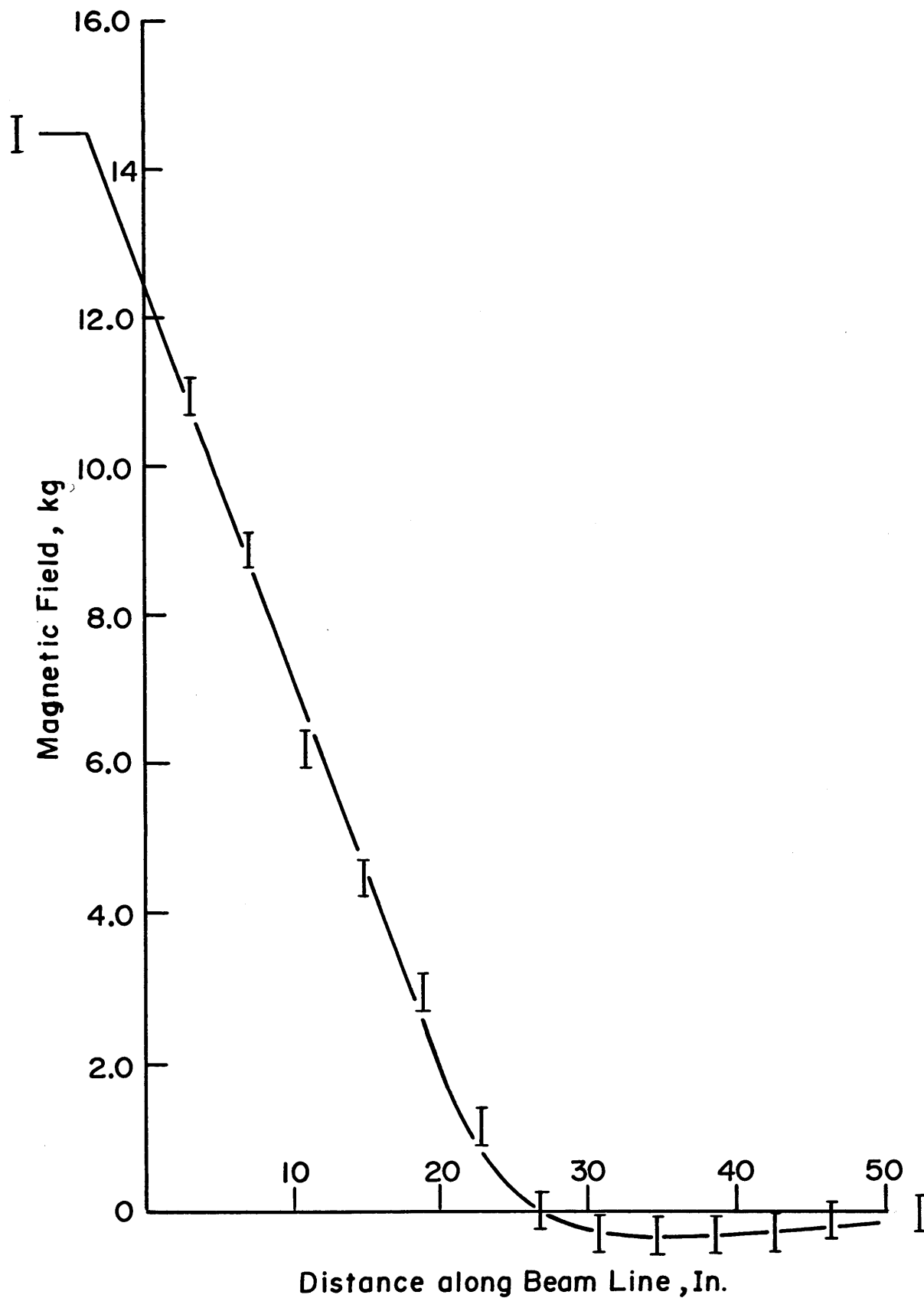
Magnetic Field, kg

Distance along Beam Line, In.

<u>Figure IV</u>

Beam trajectories

This drawing shows the locations of the three beam chambers, the scintillator, S_6, and the platinum target. Superimposed are the calculated trajectories of a 2.0 GeV/c incident K^+ (the most curved line), a 3 GeV/c K^+ (the curve incident on the center of the target with zero slope), and either with the magnetic field turned off (the straight line). The distance along the beam line is scaled down a factor of ten in comparison with the perpendicular distance.
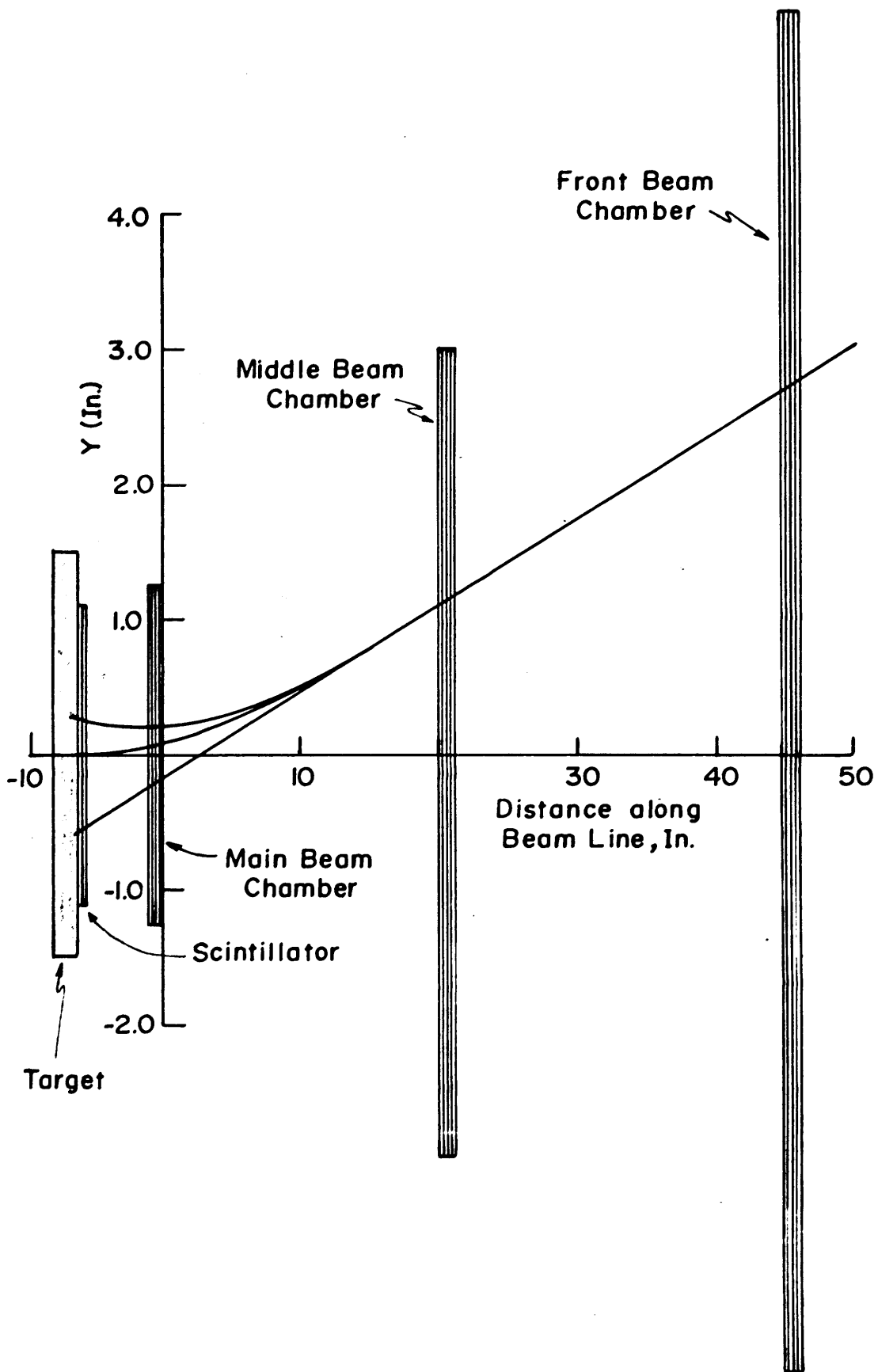
Figure V

Difference of spark location and extrapolated value

The upper curve is the calculated value of the difference

between the spark locations in the main beam chamber and that

extrapolated from the first two beam spark chambers for various

momenta and magnetic fields.

The middle curve is this difference as measured for these

various parameters for beam particles which were observed

downstream to verify their momenta.

The lower curve is this difference as plotted for Ke_3

and K^o data.

-0.6   -0.4   -0.2   0.0   0.2   0.4

Data from
Section IX
and X

Data from
Section VIII

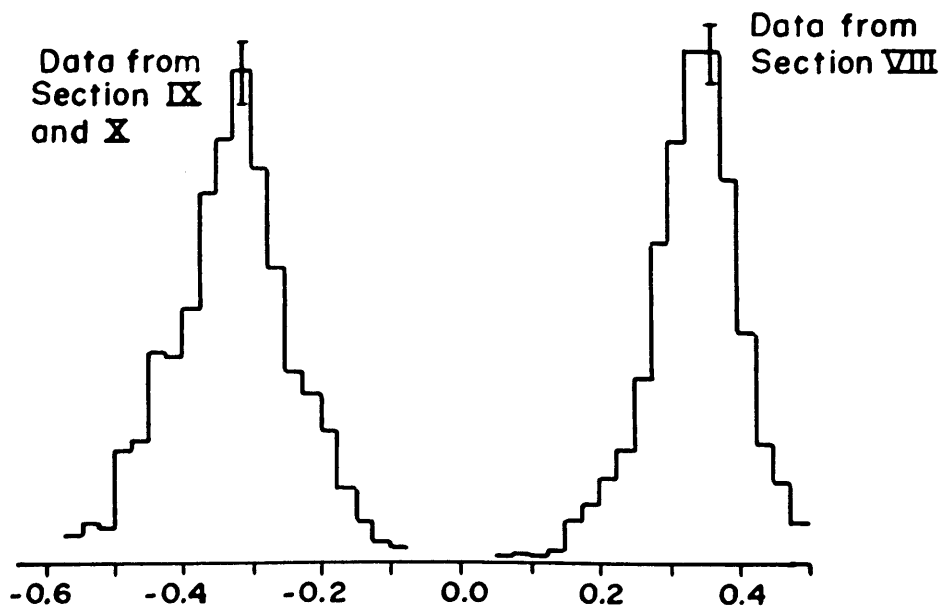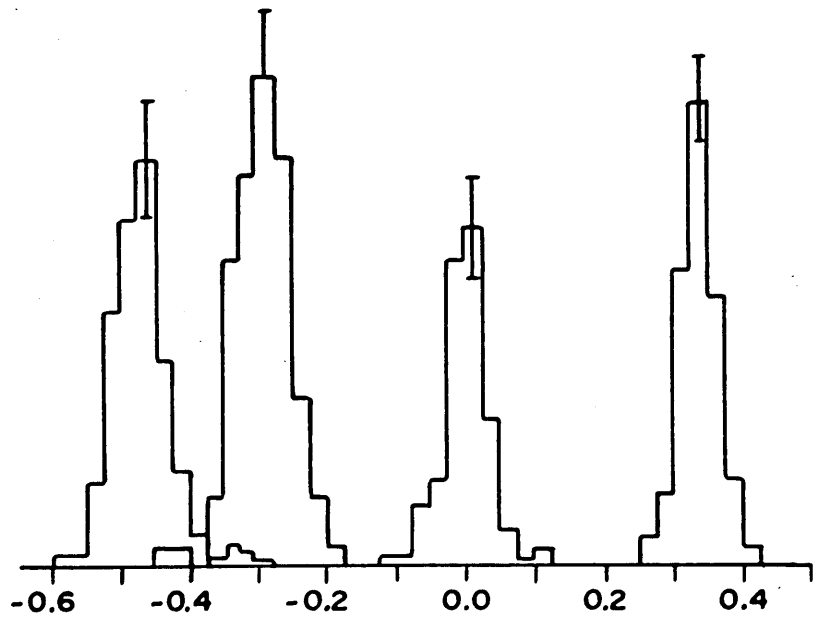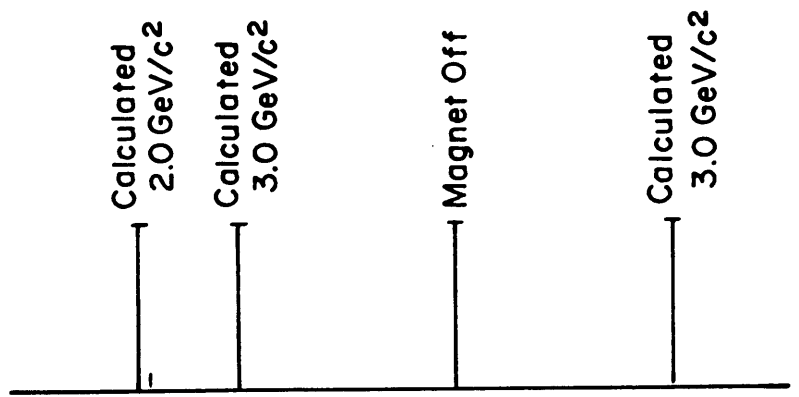-0.6   -0.4   -0.2   0.0   0.2   0.4

Figure VI

Scintillator-target complex

This figure shows two views of the scintillation counter S_6, the platinum target, and the veto scintillation counter downstream of the target.

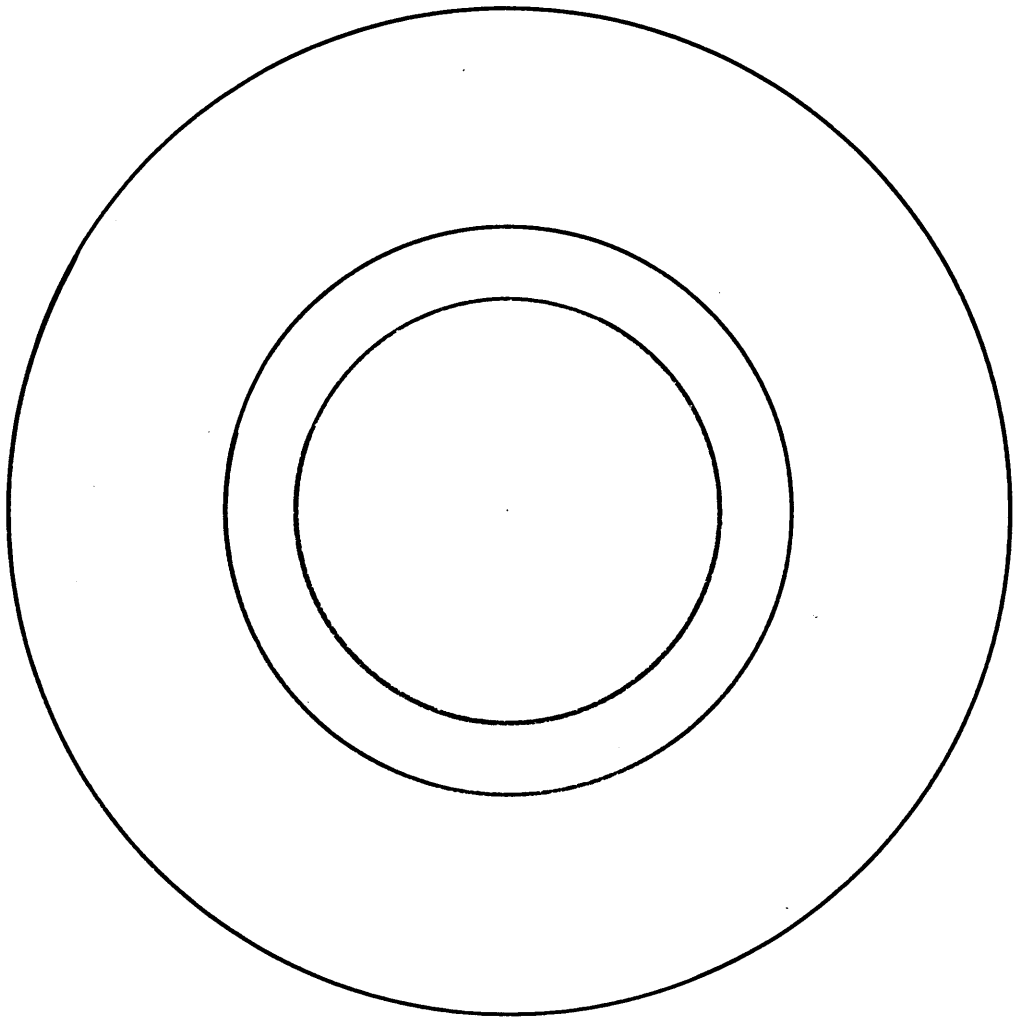The scale of this figure is actual size.

Figure VII

Momentum of the K^o in the laboratory for

platinum target

The dashed curve represents the momentum of the K^o as

measured. The solid curve is the momentum spectrum corrected for

geometric efficiency.

Momentum of Outgoing K°
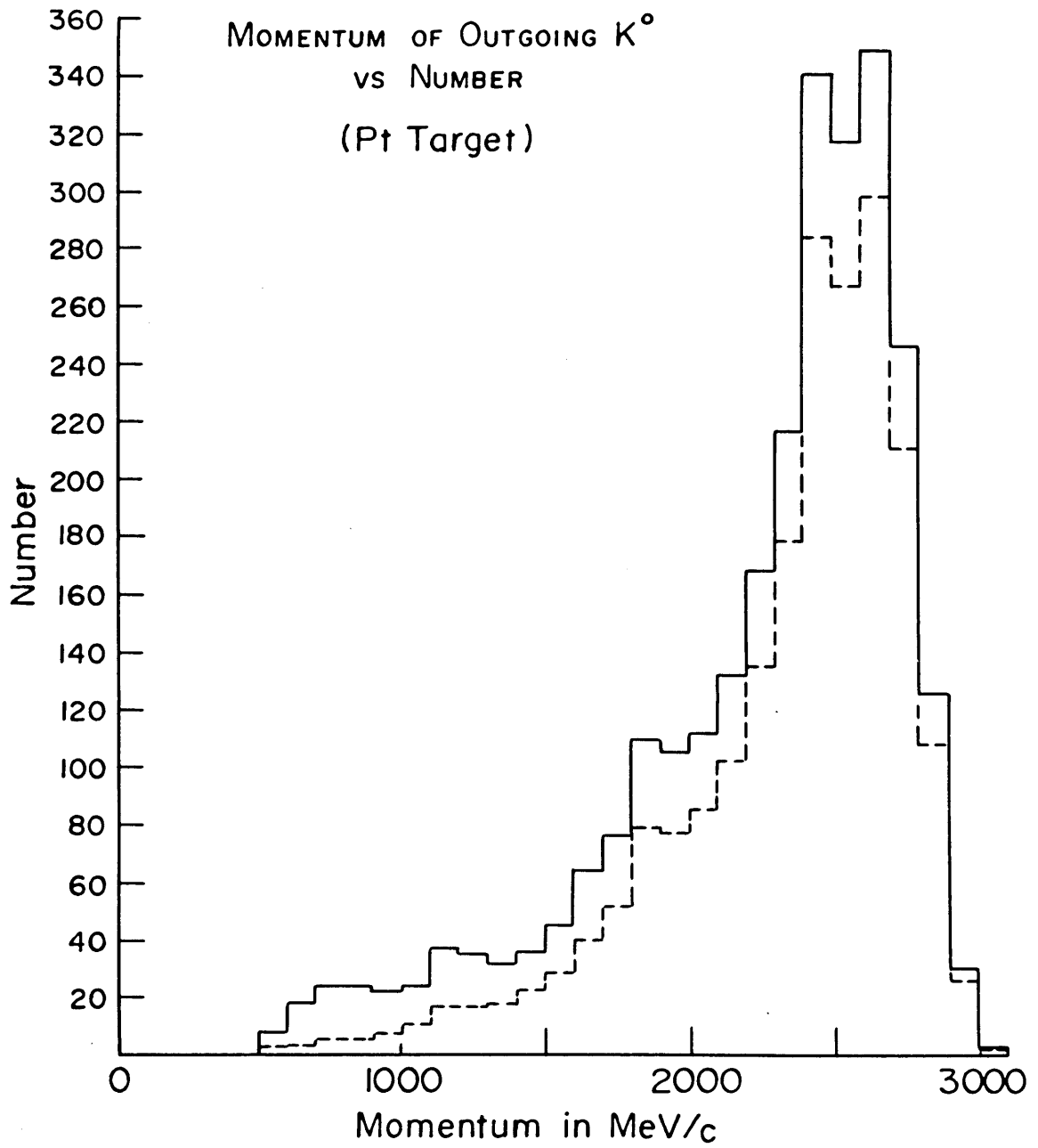vs Number

(Pt Target)

Momentum in MeV/c

Figure VIII

Momentum of the K^o in the laboratory for

target empty

The dashed curve is the momentum spectrum as measured.

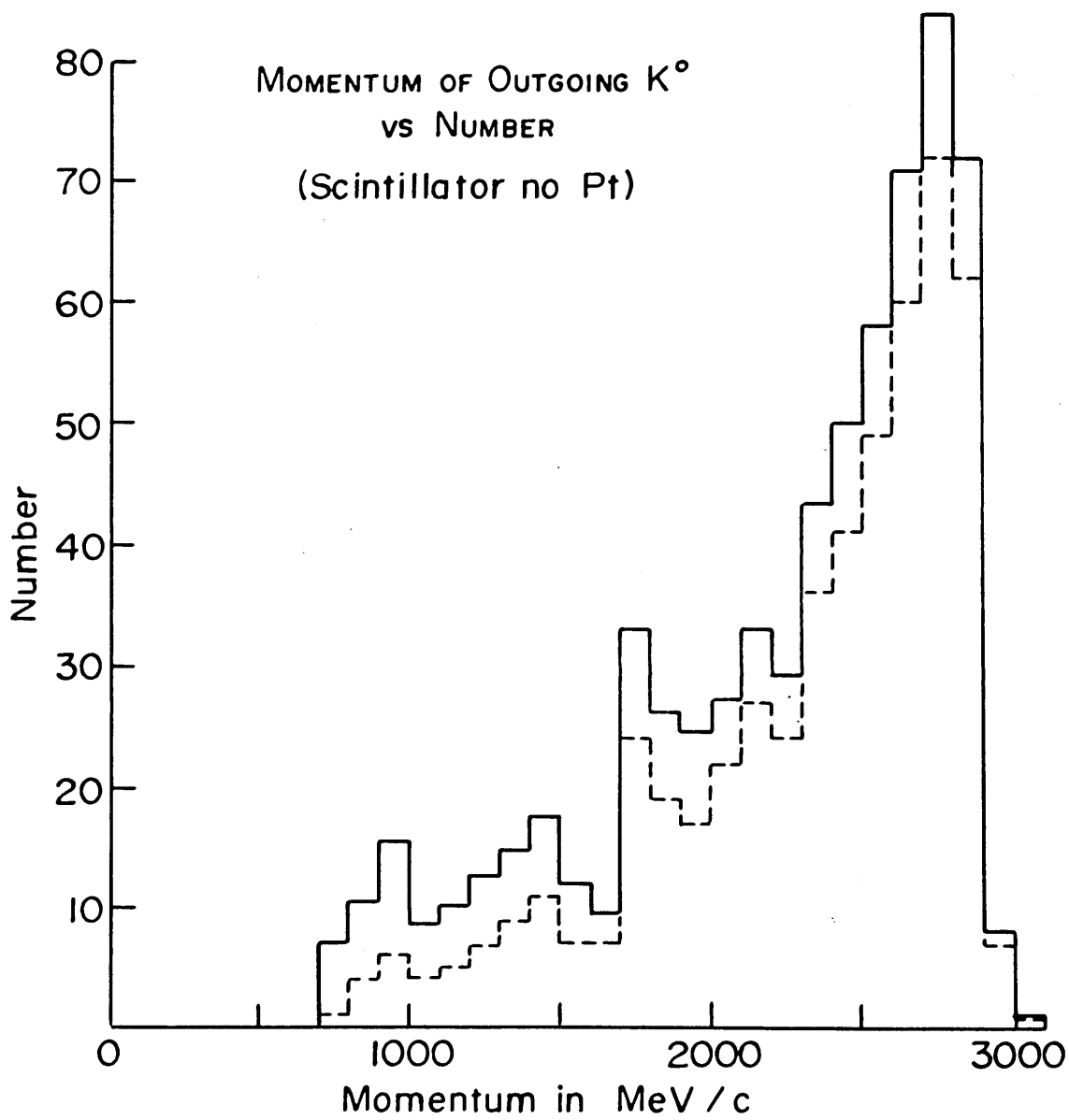The solid curve is the momentum spectrum corrected for geometry.

MOMENTUM OF OUTGOING K°
vs NUMBER

(Scintillator no Pt)

Figure IX

Angular distribution of the K^o for

platinum target

The short-dashed curve is the laboratory angular distribution
as measured. The solid curve is this angular distribution as
corrected for geometric efficiency. The long-dashed curve represents
what isotropic in the laboratory would be when normalized for the
region 0.0 to 0.52 radians.

K° TARGET FULL

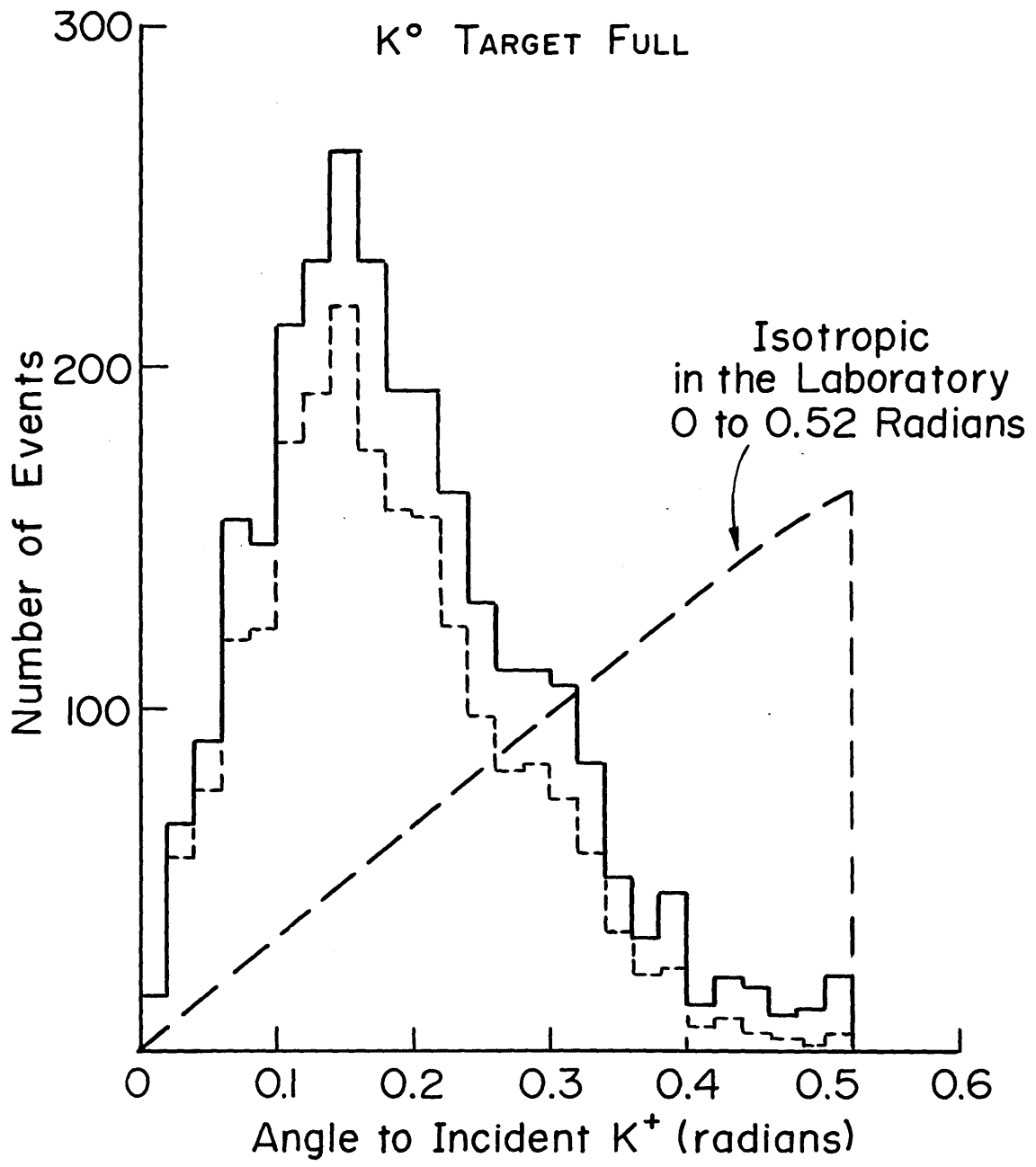Isotropic in the Laboratory 0 to 0.52 Radians

Figure X

Angular distribution of the K^o for

target empty

The dashed curve is the laboratory angular distribution as measured. The solid curve is this angular distribution as corrected for geometric efficiency.
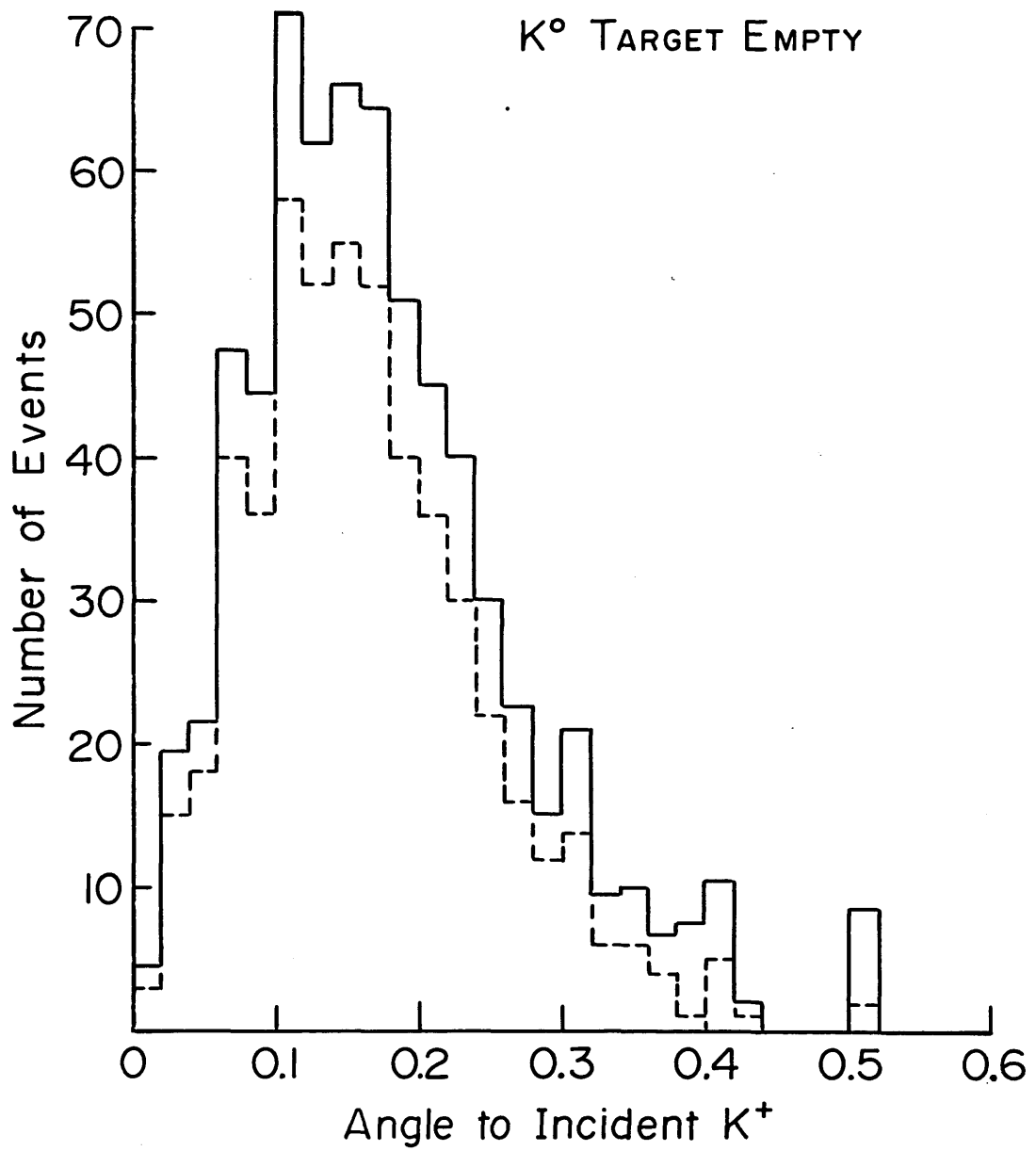
Figure XI

Differential cross-section for

platinum target

This figure is a plot of $\frac{d\sigma}{dt}$ versus t. The points with error bars represent the differential cross-section as measured, while the x's represent the differential cross-section after correction for geometric efficiency.
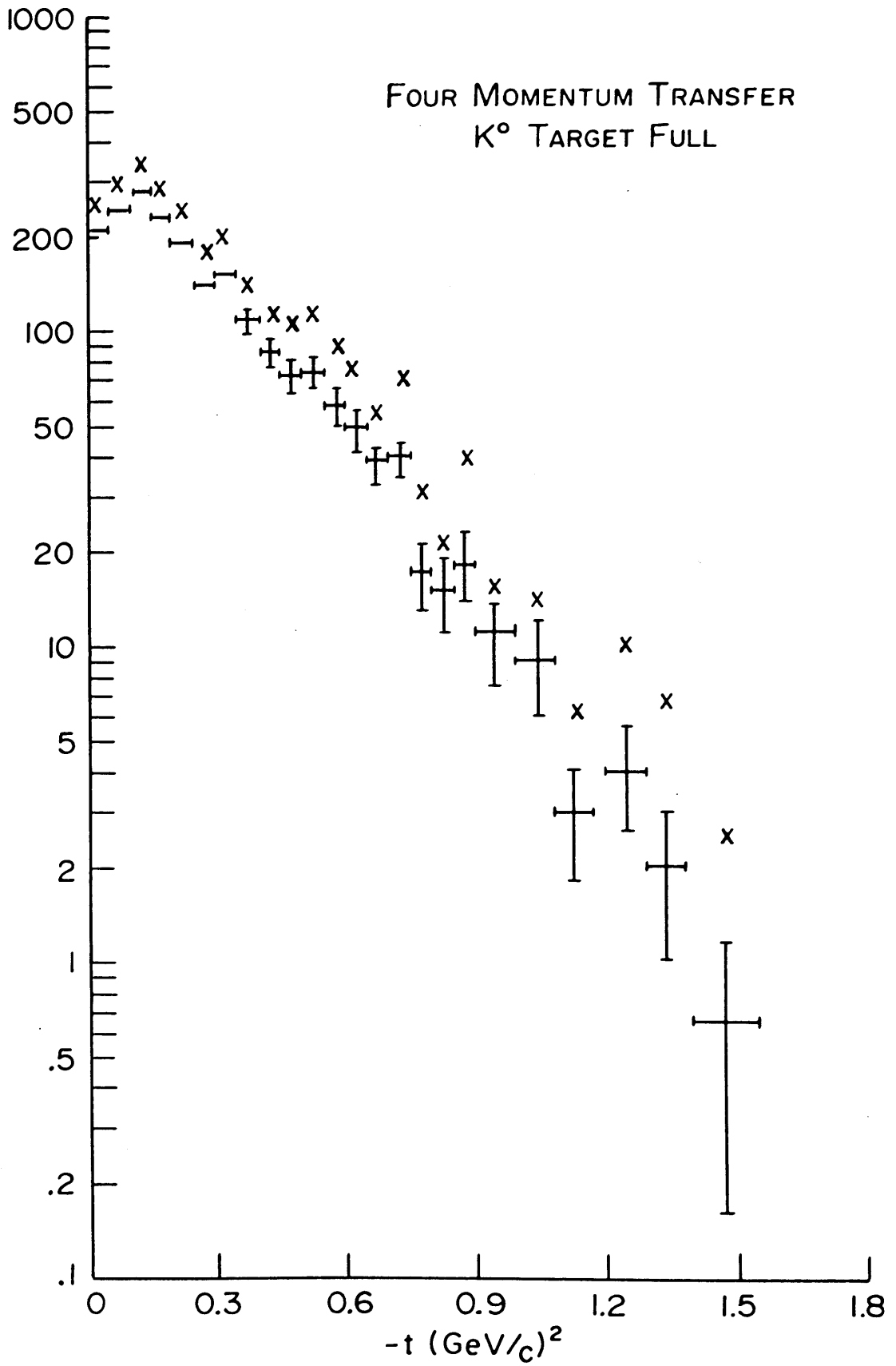
Four Momentum Transfer
K° Target Full

−t (GeV/c)²

Figure XII

Differential cross-section for

target empty

This figure is a plot of $\frac{d\sigma}{dt}$ versus t. The points with error bars represent the differential cross-section as measured, while the x's represent the differential cross-section after correction for geometric efficiency.

Four Momentum Transfer
K° Target Empty

73.

Figure XIII

K^o Momentum distribution for Monte Carlo

generated $K^+ + n \rightarrow K^o + p$

The solid curve represents the momentum spectrum calculated

for $K^+ + n \rightarrow K^o + p$, with the neutron in platinum. The

dashed curve represents the momentum spectrum calculated for the

above process with an additional elastic scattering. The two

curves are normalized for what is expected when using platinum.

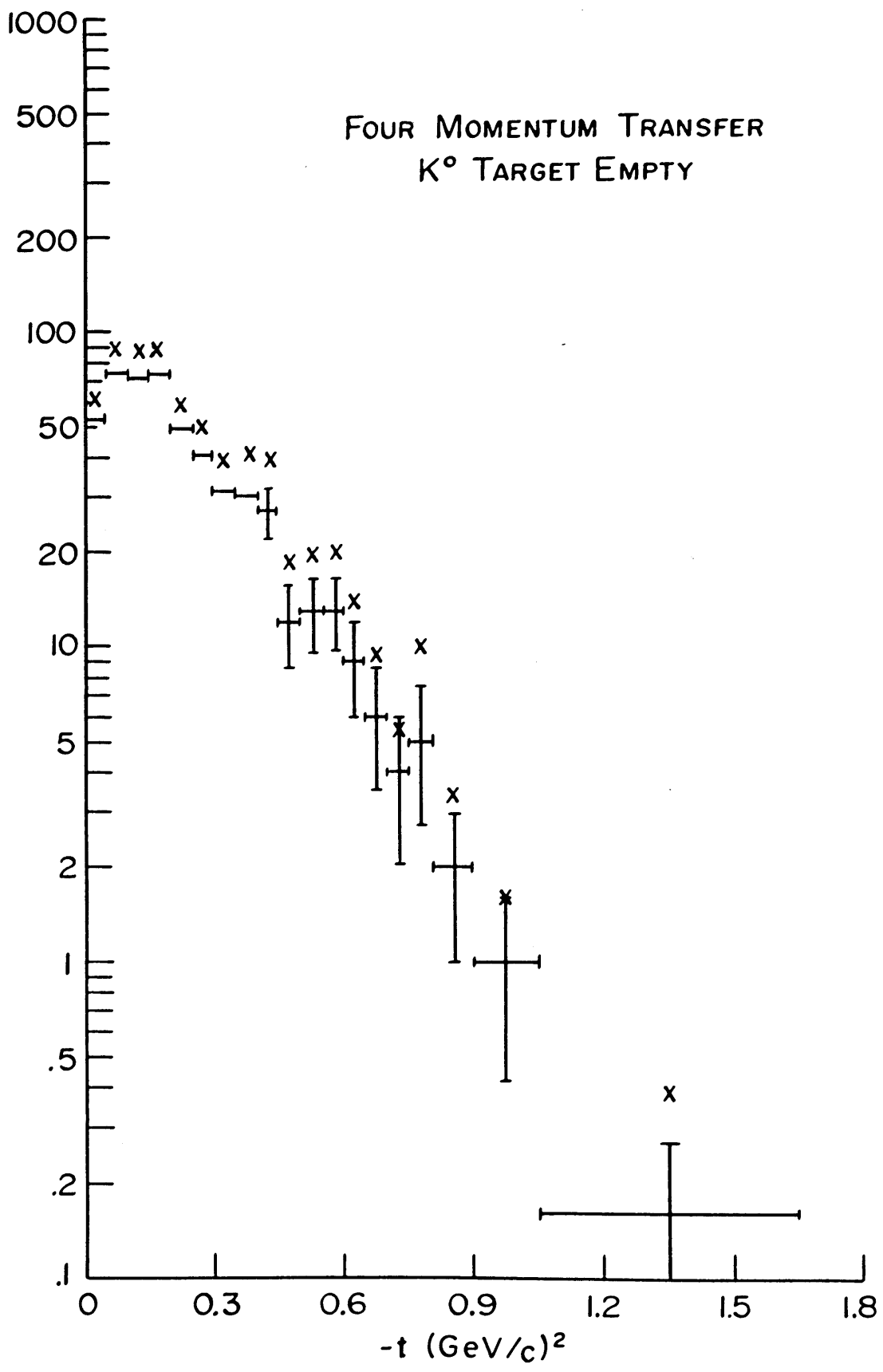K$^+$ + n $\longrightarrow$ K$^{\circ}$ + p

Figure XIV

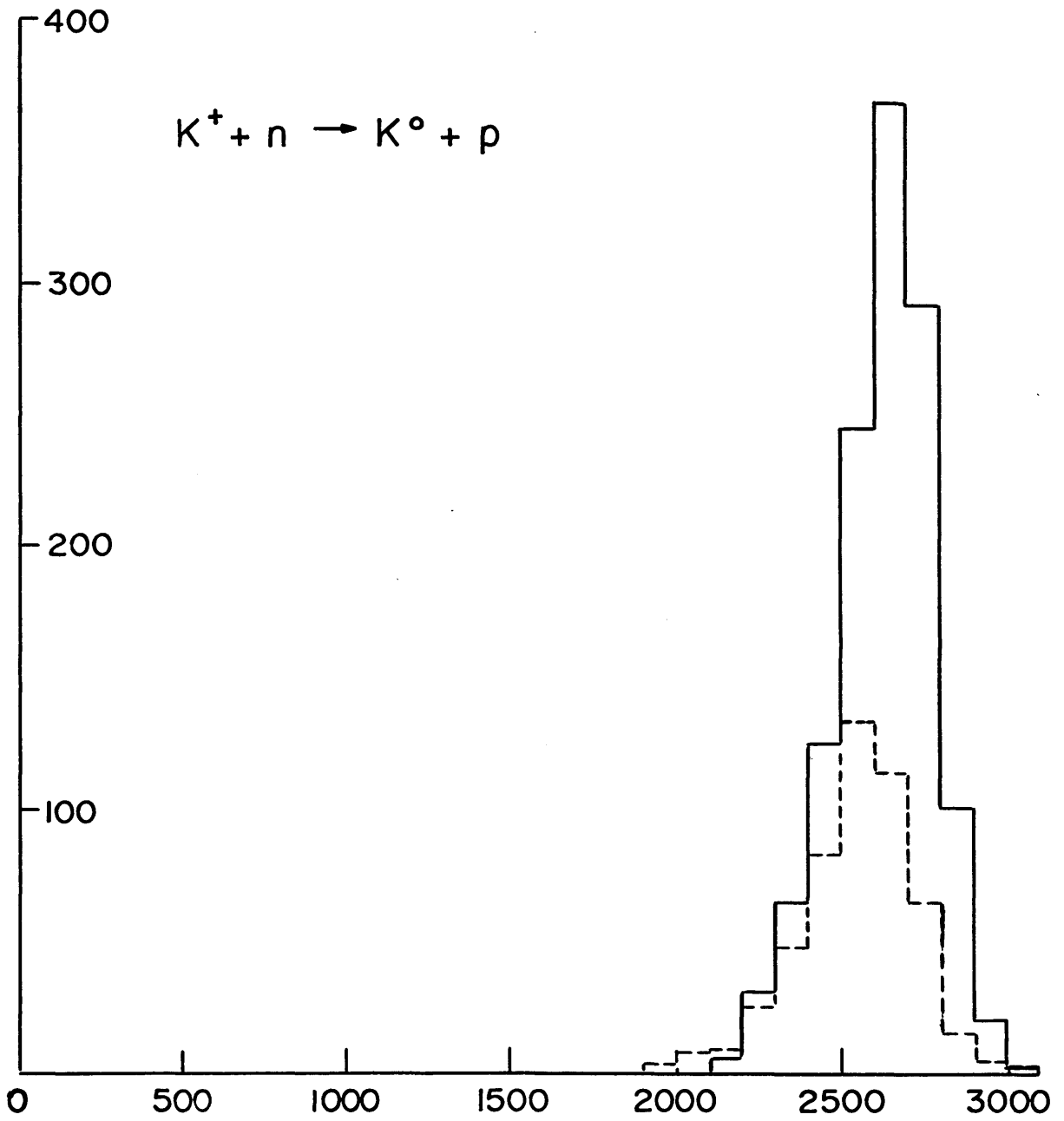K^o momentum distribution for Monte Carlo

generated $K^+ + n \rightarrow K^o + \Delta^+$ (1236)

The solid curve represents the momentum spectrum calculated

for $K^+ + n \rightarrow K^o + \Delta^+$ (1236) and the dashed curve represents this

reaction with either kaon undergoing an additional scattering.

This calculation was done for platinum.

$K^+ + n \longrightarrow K^{\circ} + \Delta^+$
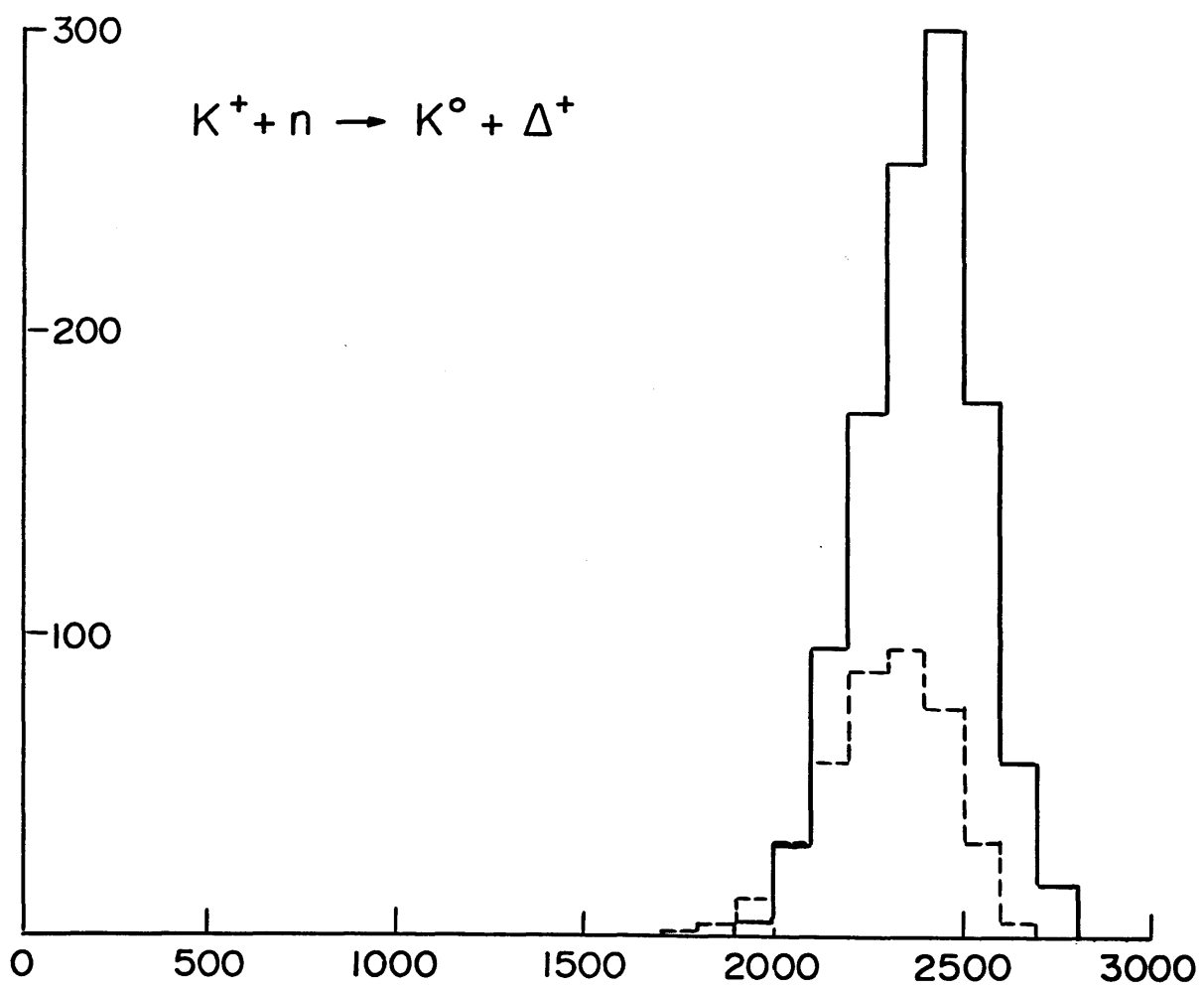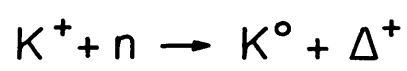
Figure XV

K^o momentum distributions for various Monte Carlo

generated $K^+ + n$ interactions

The upper curve represents the K^o momentum spectrum in the laboratory for the reaction $K^+ + n \rightarrow K^o + N^* + \pi$. The center curve represents the K^o momentum spectrum for the reaction $K^+ + n \rightarrow K^o + N^*$ including $KN\pi$ phase space. The lower curve represents the K^o momentum spectrum as calculated for the reaction $K^+ + n \rightarrow K^* + p \rightarrow K^o + \pi^o + p$. It is shown scaled up a factor of three relative to the other curves.

$K^+ + n \rightarrow K^\circ + N^* + \pi$

$K^+ + n \rightarrow K^\circ + N^{*\prime}s$

$K^+ + n \rightarrow K^* + p \quad x\ 3$
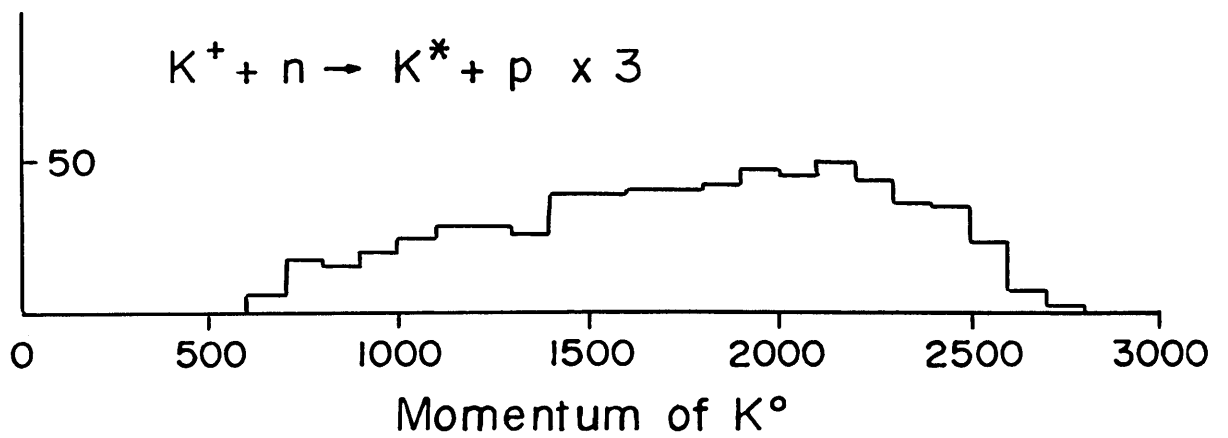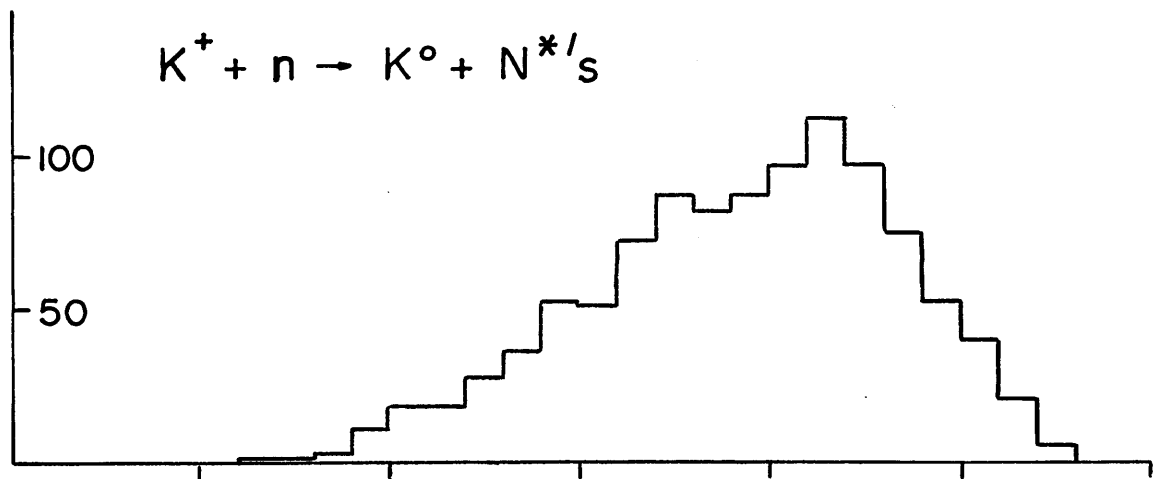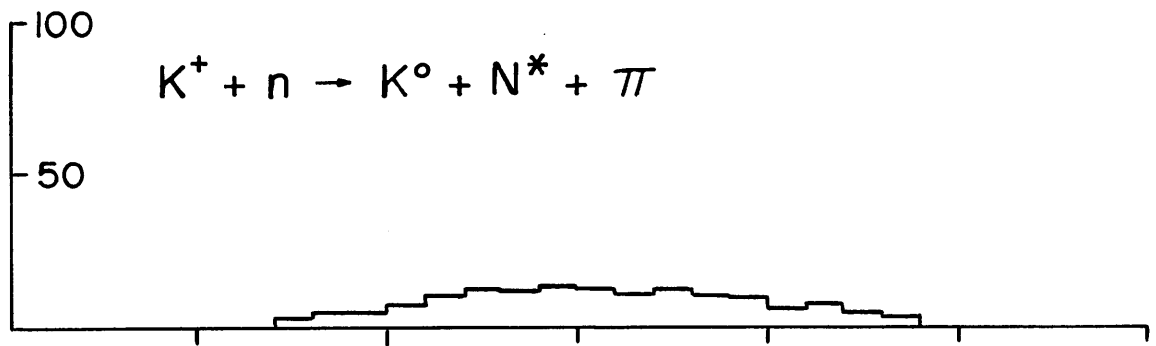
Momentum of K°

Figure XVI

Monte Carlo estimate of K^o momentum spectrum I

The solid curve represents the K^o momentum distribution in the laboratory as measured for the platinum target. The dashed curve represents the Monte Carlo estimate where it was assumed that the products $K^o p$ and $K^o \Delta^+$ had the same veto rate.

Momentum of the K$^+$ (MeV/c)
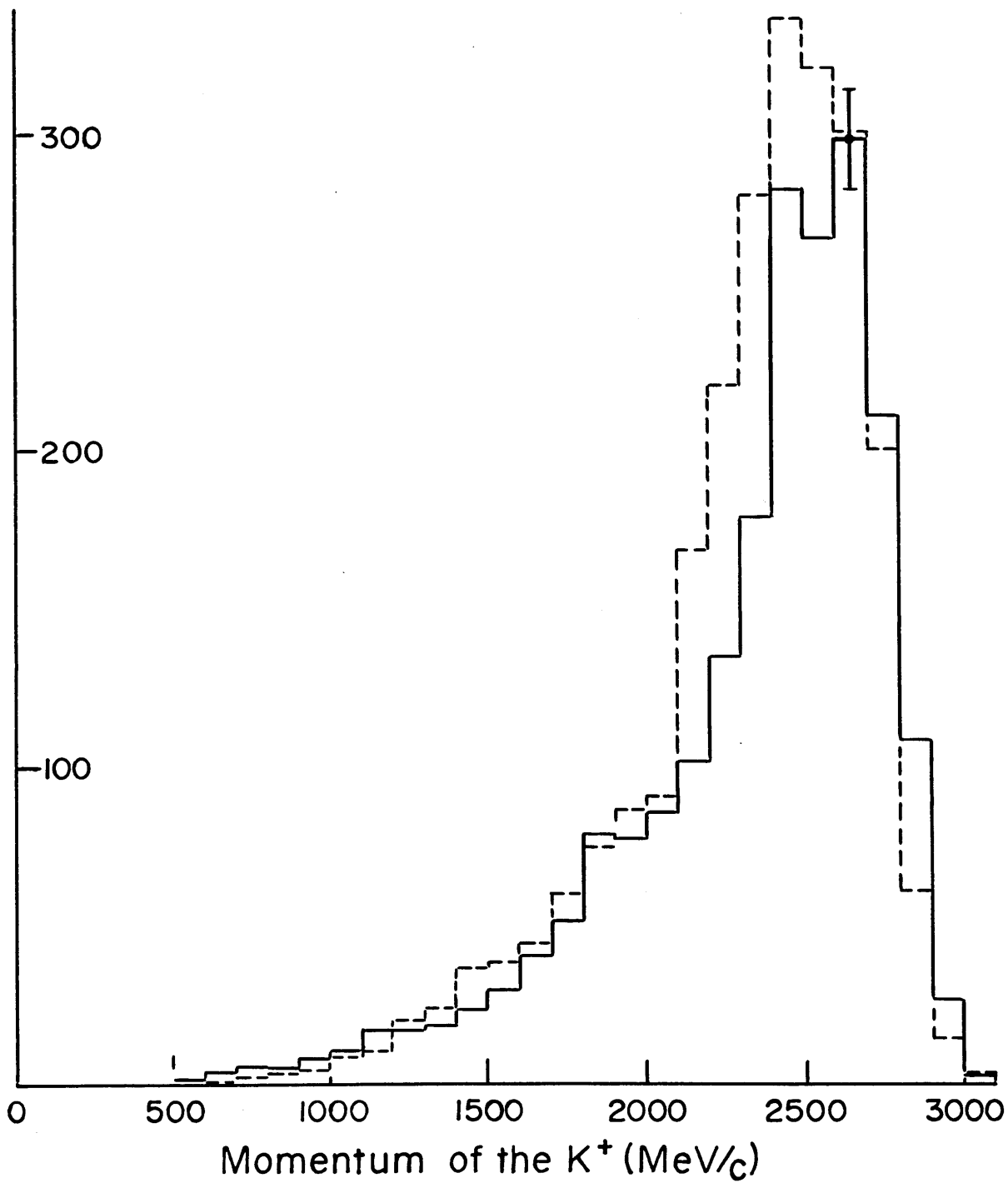
Figure XVII

Monte Carlo estimate of K^o momentum spectrum II

The solid curve represents the K^o momentum distribution in the laboratory as measured for the platinum target. The dashed curve represents the Monte Carlo estimate with $K^o \Lambda$ component suppressed by 25% relative to Figure XVI.

Momentum of the K° (MeV/c)
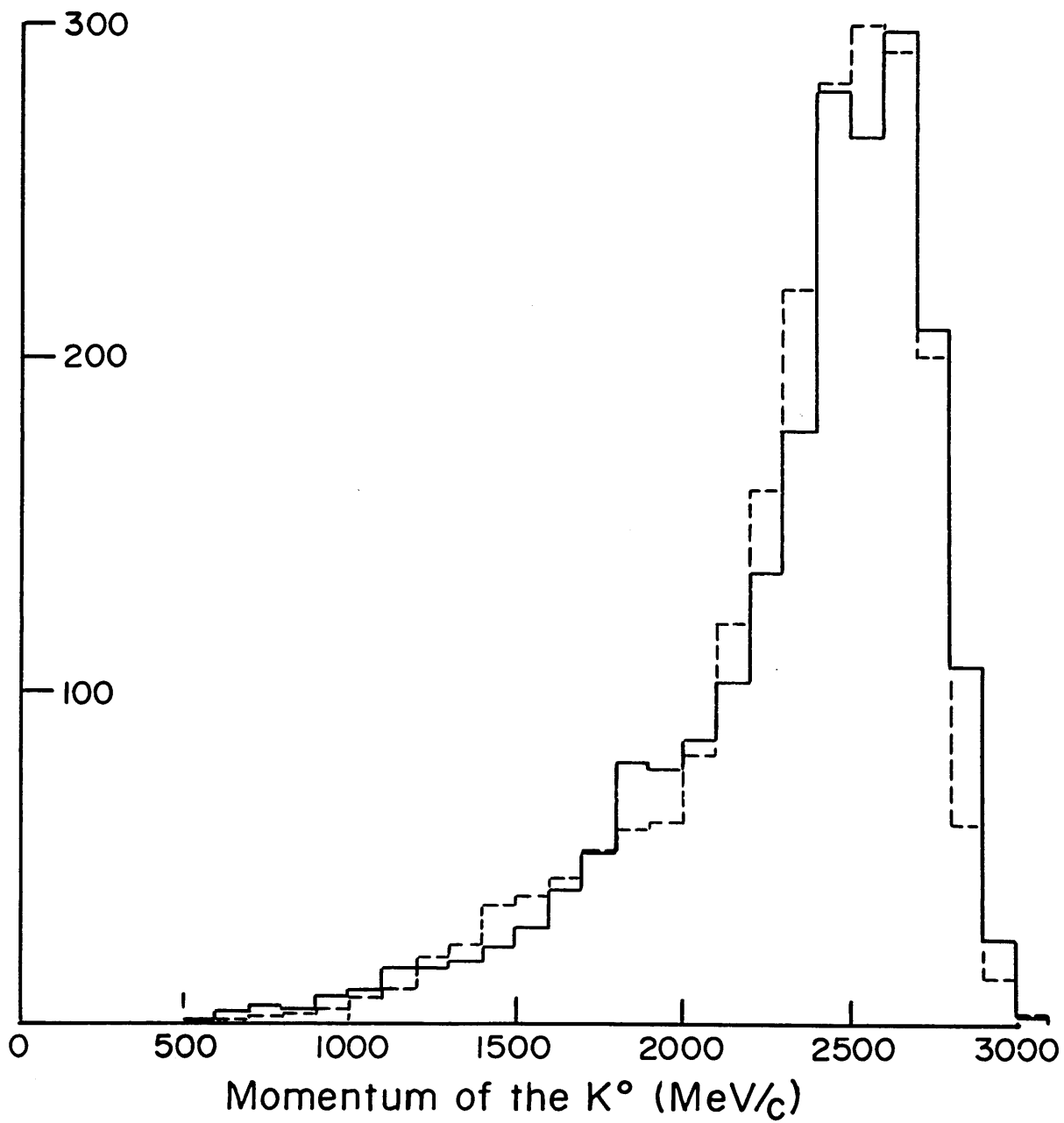
Figure XVIII

Missing mass spectrum for the

platinum target

The figure is a plot of the number of events as a function

of missing mass for the data taken on the platinum target with

a K^o trigger.

K° Platinum Target

Missing Mass (MeV/c²)
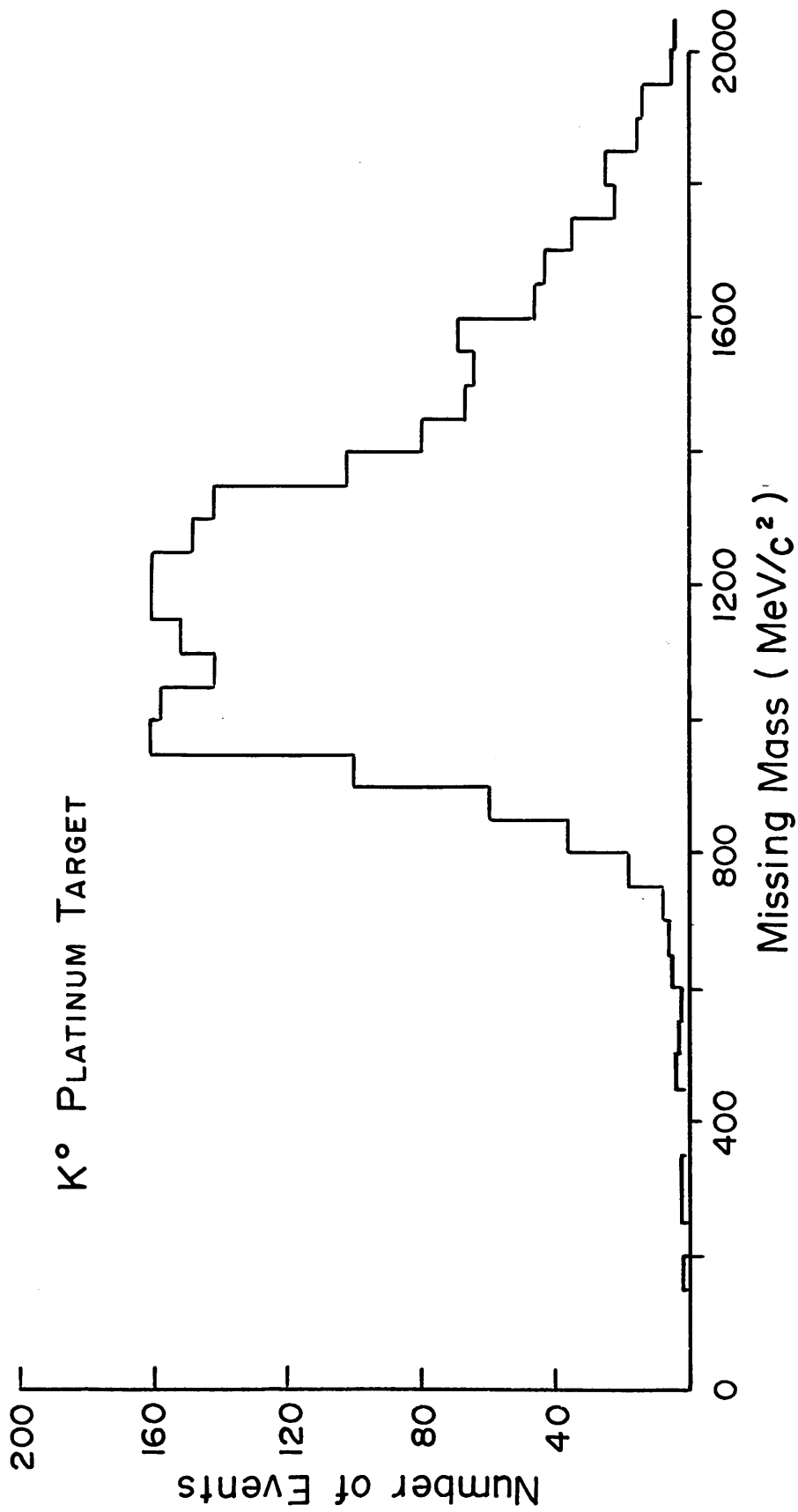
Number of Events

Figure XIX

Missing mass spectrum for target empty

This figure is a plot of the number of events as a function of missing mass for the data taken with the target empty and with a K^o trigger.
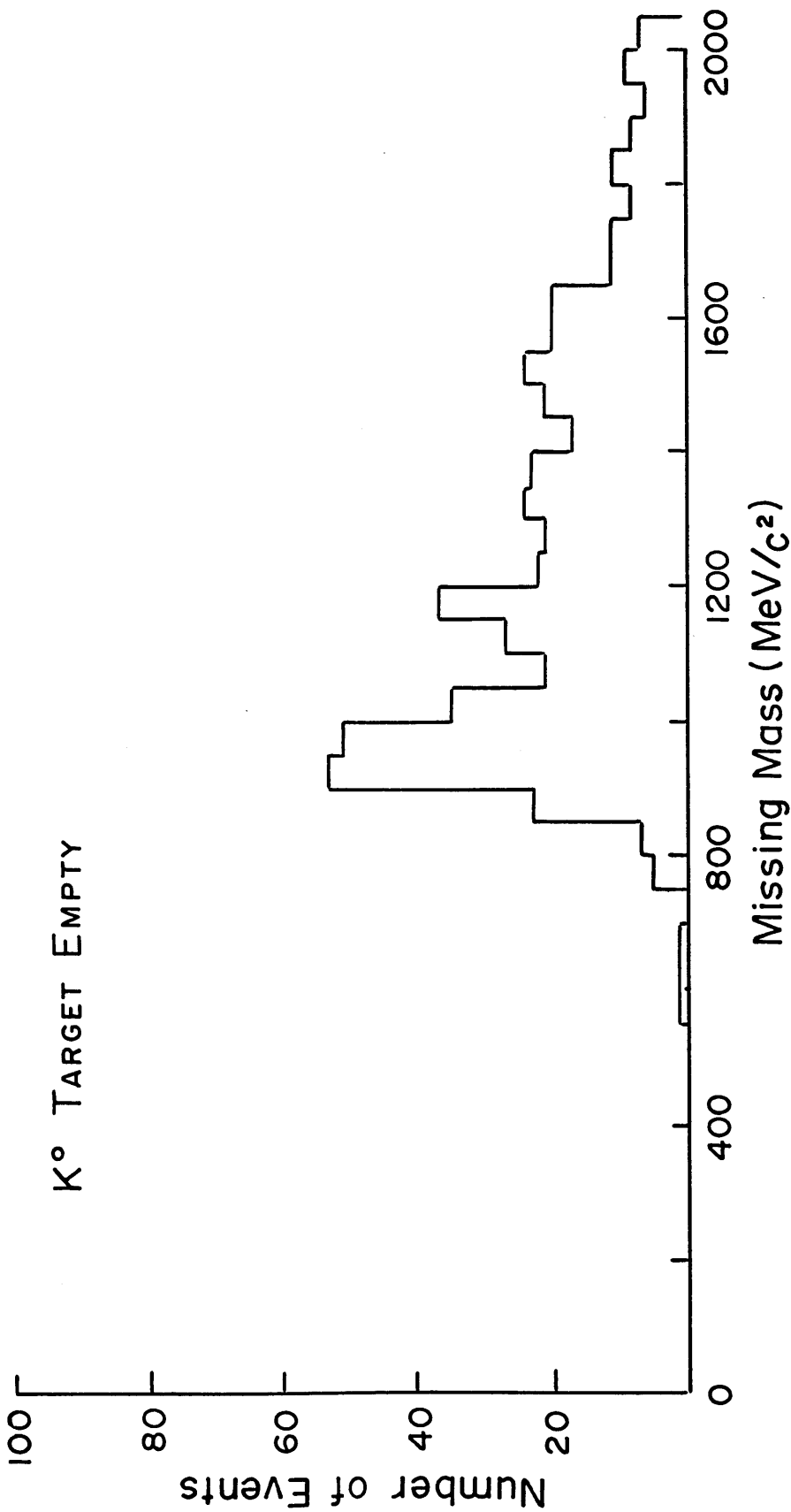
Figure XX

Missing mass spectra for Monte Carlo

generated $K^+ + n \rightarrow K^o + p$

The solid curve is the missing mass spectrum for $K^+ + n \rightarrow$ $K^o + p$ as calculated by the Monte Carlo program. The dotted curve is the missing mass spectrum for this reaction when a kaon also undergoes another scattering.
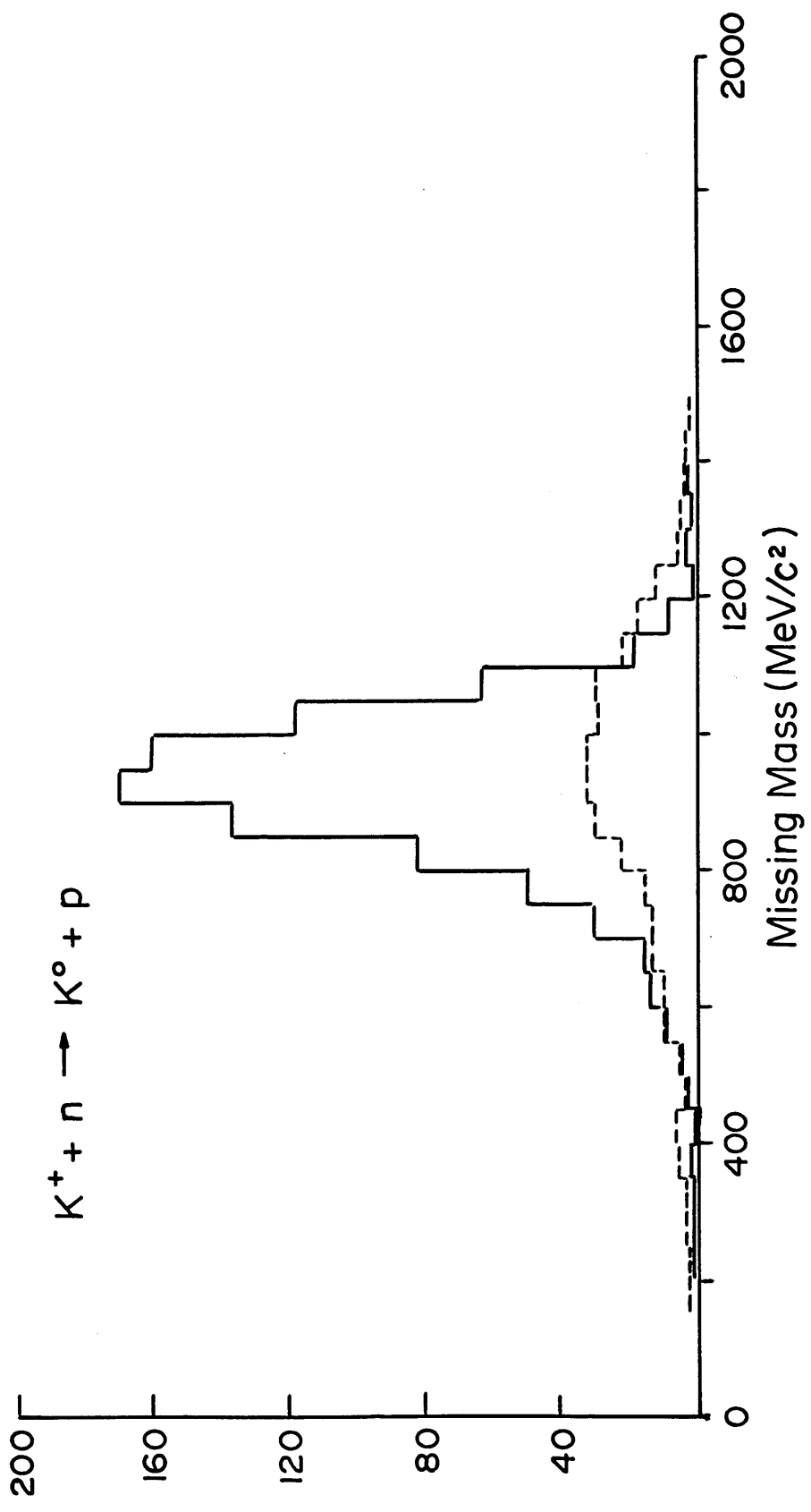
Figure XXI

Missing mass spectra for Monte Carlo
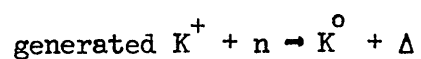
generated $K^+ + n \rightarrow K^o + \Delta$

The solid curve is the missing mass spectrum for $K^+ + n \rightarrow$ $K^o + \Delta$ as calculated by the Monte Carlo program. The dotted curve is the missing mass spectrum for this reaction when a kaon also undergoes another scattering.

$K^+ n \longrightarrow K^\circ + \Delta^+$
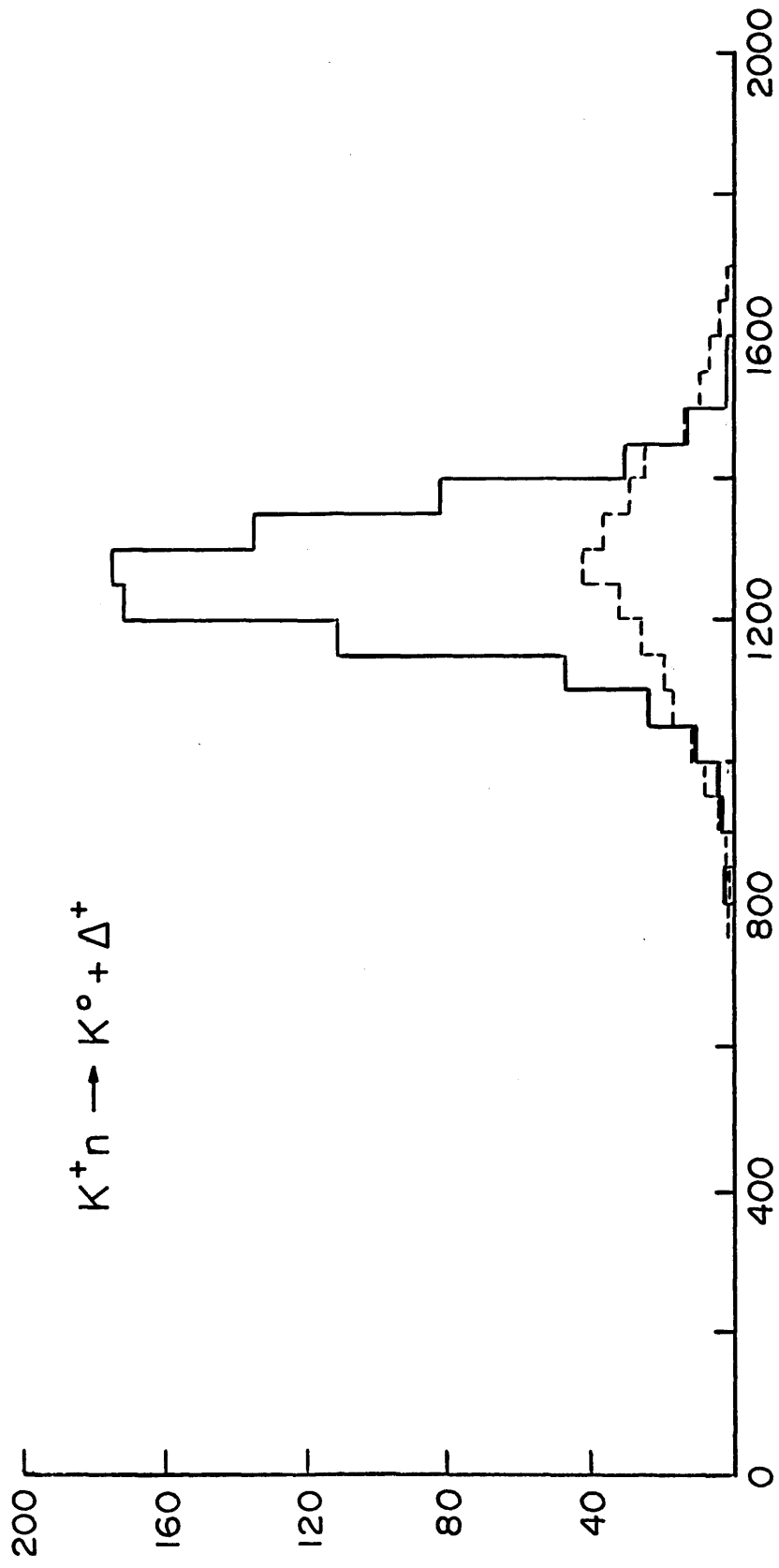
References

1.   O. Fackler, M.I.T. Ph.D. Thesis, 1969.

2.   A.S. Goldhaber and C.J. Joachain, "High-energy Hadron-Nucleus Collision, I. Protons", Phys. Rev. 171, 1566, (1968).

3.   "A Compilation fo K^+N Reactions", UCRL - 20,000 K^+N, Sept., 1969.

4.   Goldhaber and Joachain, loc. cit.

5.   J.M. Wilcox and B.J. Mayer, "Nuclear Internal Momentum Distributions", Phys. Rev. 99, 875, (1955).

6.   J.B. Cladis, et al., "Nuclear Momentum Distributions in Deuterium and Carbon Inferred from Proton Scattering", Phys. Rev. 87, 425, (1952).

7.   J. Heidmann, "The Production of High Energy Deuterons by Energetic Nucleons Bombarding Nuclei", Phys. Rev. 80, 171, (1950).

8.   M.L. Goldberger, "The Interaction of High Energy Neutrons on Nuclei", Phys. Rev. 74, 1269, (1948).

9.   J.M. Miller and J. Hudis, "High Energy Nuclear Reactions", Annual Review of Nuclear Science, Vol. 9, 1959.

10.   Goldhaber and Joachain, loc. cit.

11.   R.J. Glauber, "Theory of High-Energy Hadron-Nucleus Collisions", Review talk presented at the Third International Conference on High Energy Physics and Nuclear Structure, Columbia University, Sept. 9, 1969.

12.   Y. Goldschmidt-Clermont, et al., "K^+n Charge Exchange Reaction at 3 GeV/c", Phys. Letters, 27B, no. 9, 602, (1968).

13.   A.M. Boyarski, et al., "Single π^+ and K^+ Photoproduction Complex Nuclei at 8 and 16 GeV/c", Phys. Rev. Letters, 23, 1343, (1967).

14.   G. Bassompierre, et al., "Production of K^+ (892) in K^+N
       Interactions at 3 GeV/c", Nuclear Physics, B16, 125,
       (1970).

15.   J.F. Martin, M.I.T., Ph.D. Thesis.

APPENDIX A

OPTICAL CONSTANTS

The Outer Optics

The spark chambers and their satellite mirrors were viewed by an outer optical system consisting of a parabolic mirror, a kick-out mirror, an aperture, and a rapid advance 35 mm camera.
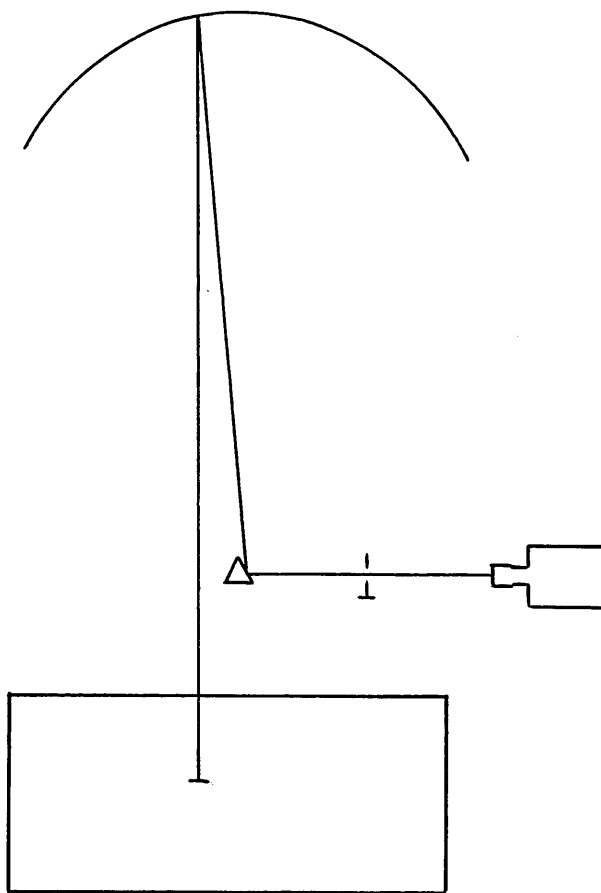
The function of this outer optics was to take vertical light rays from objects in the field of view and to focus them on the film in the camera. This outer optical system was calibrated by using it

to photograph a large precision grid (± 1 mil absolute accuracy of location) at several heights with the magnetic field on and off. The data from these photographs were analyzed by J. F. Martin; he found that in order to reconstruct the actual location of an object in the fiducial volume, one should follow this procedure:

First, apply an R^2 correction, which is characteristic of parabolic mirrors

$$X_I = (A + C \cdot R^2) \, X_M$$

$$Y_I = (A + C \cdot R^2) \, Y_M$$

where R is the distance of the object from the optical axis, and A and C are constants. This formula converts measurements from microns on film to inches in real space.

Then, if

$$W = (X_I - 4.5) \times \cos\Phi + (Y_I + 2.5) \sin\Phi = 0.4$$

one has

$$X = X_I + 3.3 \times 10^{-5} W^2 - 0.0043$$

$$Y = Y_I - 1.0 \times 10^{-4} \times Y_I{}^2 + 0.0057.$$

This procedure for reconstructing film measurements to real space coordinates reproduces the coordinates of the grid consistent with the accuracy of film measurement with no apparent systematic distortion [15].

Chamber Seven

Seven of the eight momentum analysis spark chambers were viewed

directly by the outer optics and so were thought to need no further

correction for their top view. This hypothesis was found to be

valid to an accuracy of ± 1 mil by least square fits to straight

lines, circles (particle trajectories), and fiducial light measure-

ments.

However, the seventh chamber was viewed through a pair of

shiftover mirrors.
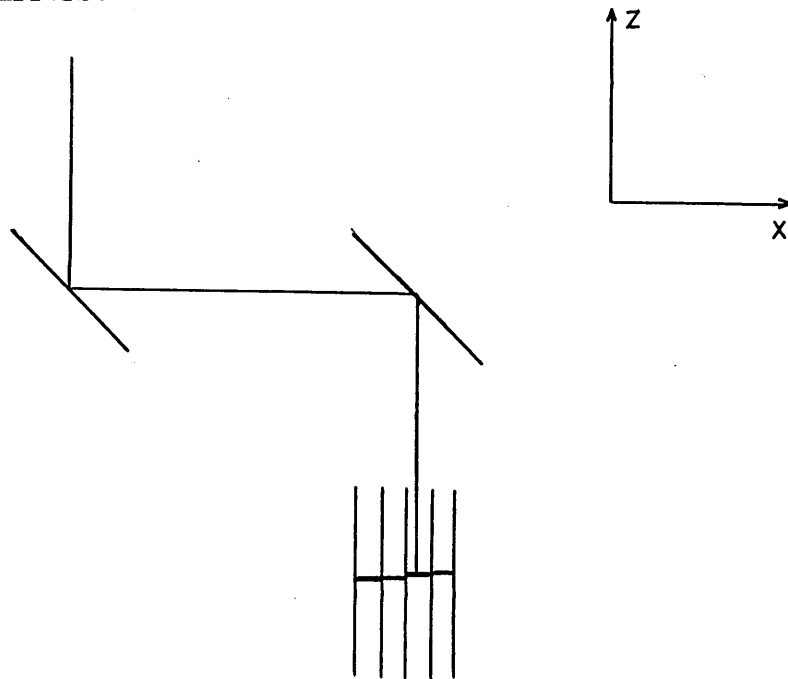
Because of these shiftover mirrors, an additional correction beyond

the outer optics is needed.

When the mirrors were installed, an attempt was made to have the

following relationship between the apparent position X_M, Y_M and the

actual position X,Y:

$$X = X_M + 6.0"$$

$$Y = Y_M \; ;$$

however, the side view of chamber seven was partially obscured by the shiftover mirror. A compromise was made by rotating and shifting the mirror support so that

$$X = \cos\theta \; X_M + \sin\theta \; Y_M = 6.2"$$

$$Y = -\sin\theta \; X_M + \cos\theta \; Y_M + 0.125$$

would represent the relationship between apparent and actual position.

If we allowed all degrees of freedom for these plane mirrors, the relationship would be

$$X = B_X X_M + B_Y Y_M + B_Z Z_M + D_X$$

$$Y = C_X X_M + C_Y Y_M + C_Z Z_M + D_Y$$

Using measurements of the fiducial lights and measurements of particle trajectories (requiring all four sparks to appear in chambers six, seven, and eight to remove any systematic errors from souces such as the E cross B and high voltage spark drift), the parameters of the full free relationship were computed. They were:

SECTION NUMBER	C_Y	C_X	C_Z	D_Y
1	1.003	0.002	-0.003	-0.003
2	1.003	0.003	-0.003	-0.005
3	1.003	0.003	-0.003	-0.003
4	1.002	-0.007	-0.003	-0.003
5	1.003	-0.006	-0.003	-0.008
6	1.003	0.005	-0.003	-0.005
7	1.002	0.004	-0.003	-0.006
8	1.003	0.005	-0.003	-0.006
9	1.002	-0.009	-0.003	-0.006
10	1.003	-0.005	-0.003	-0.008
ESTIMATED ERROR	±0.0003	±0.0005	±0.0003	±0.001

These constants appear to be very good as judged in comparison to

the measurements of spark image location with fitted trajectories.

Distance from Spark to Fitted Trajectory in Mils

There is no systematic variation of the fit with X, Y, or Z.

After achieving this internal consistency, a study was made to see what effect a variation in these constants would have on the dipion mass.

First, these constants were set to their ideal values, i.e. C_Y equal one, and C_X, C_Z, and D_Y equal zero. The data were analyzed with the constants and each event's mass compared to its mass value with the constants at their computed values. The result was that the differences had a standard deviation of less than one MeV/c^2 and 90% of the events had new masses less than 5 MeV/c^2 from their old value. Similar results were found by varying the constants an equal amount in the other direction. Next, the individual constants were varied and the following was found:

$$\Delta CY = 0.01 \quad \sigma < 1.0 \ MeV/c^2 \quad 90\% \ within \pm 10 \ MeV/c^2$$

$$\Delta CX = 0.05 \quad < 1.0 \ MeV/c^2 \quad 97\% \ within \pm 2 \ MeV/c^2$$

$$\Delta CZ = 0.01 \quad < 1.0 \ MeV/c^2 \quad 90\% \ within \pm 6 \ MeV/c^2$$

$$\Delta DY = 0.01 \quad < 1.0 \ MeV/c^2 \quad 98\% \ within \pm 4 \ MeV/c^2$$

Every one of these variations is in excess of 10 standard deviations of the estimated error in the constant, thus any reasonable error in these constants will not affect the mass resolution.

Side View

The outer optics looked down upon the momentum analysis spark chambers directly and looked into the side of each chamber by means of two 45° mirrors on each chamber.

Plan View   Side View
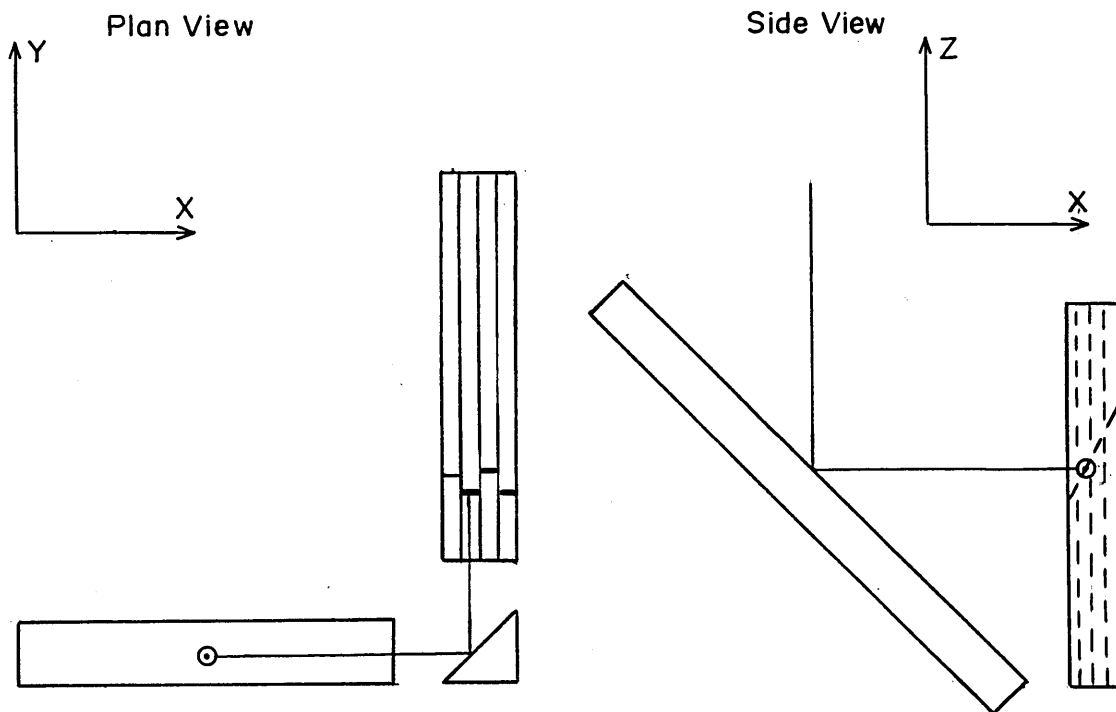
The spark chambers were originally aligned to be vertical to ± 0.1 milliradians over their full length. The two 45° mirrors were affixed and aligned so that the following relations would hold between apparent and actual locations of sparks in the chambers:

$$X = \pm \left(Y_M + D_X \right)$$

$$Z = D_Z - X_M$$

where D_X, D_Z are constants and they and the sign depend on which

chamber is under consideration. This attempt did not succeed as well

as the chamber seven attempt because there were several more degrees

of freedom. There were ten such alignments during the course of the

experiment, generated either through moving the magnet and apparatus

to change magnetic polarity or through opening the apparatus to

repair the lead plate chamber or to replace chamber five.

The assumptions that were made in calculating the side view

calibration constants were:

(1)   that the 45° mirrors were plane surfaces (this is

true to better than en effective $\pm$ 2 mils distortion

of object location except for the larger mirrors, where

it was measured to be $\pm$ 10 mils near the ends of the

mirrors).

(2)   Trajectories of particles going through the chambers

with the magnetic field off are straight lines and

with the magnetic field on they are helices.

(3)   Beam particles on the average go through horizontally.

(4)   Only vertical light rays are accepted by the outer

optics.

Procedure for Finding Spark Chamber Constants

(1) First, the side view was rotated until the gaps of the spark chamber were vertical. This should be a rotation of 90° and varied from this by less than ± 2 degrees. The following table gives the calculated value of sine of this rotation angle minus 90°. (Note that a value of zero indicates a 90° rotation.)

SECTION NUMBER	CHAMBER NUMBER							
	1	2	3	4	5	6	7	8
1	0.0	0.0033	-0.0167	0.0	-0.0230	-0.0061	-0.0028	0.0
2	0.0	0.0	-0.0150	0.0	-0.0275	-0.0060	-0.0020	0.0
3	0.0	0.0	-0.0150	0.0	.....	-0.0060	-0.0020	0.0010
4	0.0	0.0	-0.0150	0.0	.....	-0.0060	-0.0020	0.0
5	0.0	0.0	-0.0200	0.0	.....	-0.0060	-0.0020	0.0020
6	0.0	0.0	-0.0140	0.0	0.0120	-0.0060	-0.0020	0.0020
7	0.0	0.0	-0.0150	0.0	0.0125	-0.0060	-0.0020	0.0020
8	0.0	0.0	-0.0180	0.0	0.0120	-0.0060	-0.0020	0.0020
9	0.0	0.0	-0.0180	0.0	0.0140	-0.0070	-0.0025	0.0020
10	0.0	0.0	-0.0200	0.0	-0.0010	-0.0010	-0.0020	-0.0010
ESTIMATED ERROR	±0.006	±0.002	±0.0013	±0.001	±0.0007	±0.0006	±0.0005	±0.0005

In order to test the effect of an error in these angles of rotation, these rotations were varied by approximately ten standard deviations of their estimated errors and the results were that the change in

dipion mass (K-mass) was less than one MeV/c^2 for 99% of the events.

It appears the other 1% was caused by rotating the spark images out-

side of their respective gaps.

(2) At the same time that the angles of rotation were found,

the coordinates of the center of each spark chamger side view image

were determined. The x-value was determined to ~ 0.1 inch by

observing where a roughly centered fiducial light was in one section

and using this value for all sections. These values were:

CHAMBER NUMBER	F_X
1	5.295
2	8.755
3	11.325
4	13.637
5	15.629
6	17.505
7	21.472
8	24.317

The Y-value was determined for each section by observing the Y-

coordinates of all the spark images from each spark chamber. The

final requirement on the Y-value was that after the proper rotation

about the center of the chamber, the distribution of Y coordinates

be appropriately symmetrical around zero. The form of this rotation

about the center is:

$$Y = \sin\theta* \left(F_X - X_M\right) \mp \cos\theta* \left(Y_M - F_Y\right)$$

The minus sign for chambers 1-4; the plus sign
for chambers 5 - 8.

An example of this requirement is chamber 6, section 7, where the
rotation about the center would be

$$Y = -0.006* \left(17.505 - X_M\right) + 1.000* \left(Y_M - 6.140\right)$$

where X_M and Y_M are again measured spark image coordinates, produces
the following distribution:
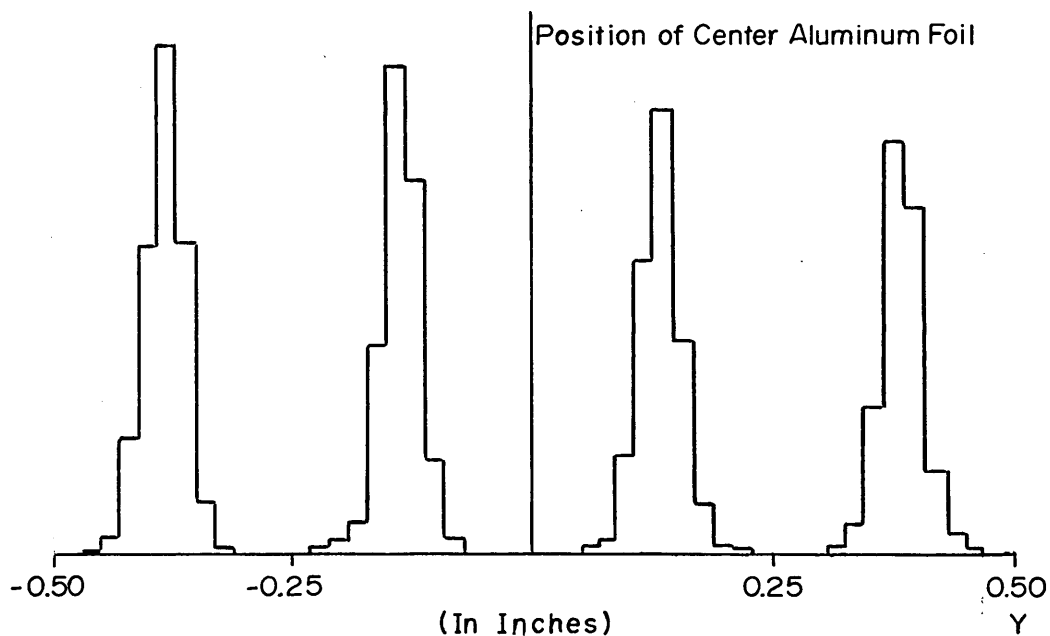
These Y-coordinates of the center of the chamber images, F_Y, are
listed in the following table:

SECTION NUMBER	CHAMBER NUMBER							
	1	2	3	4	5	6	7	8
1	23.170	24.750	26.160	27.730	7.730	6.120	4.600	3.090
2	23.200	24.765	26.200	27.765	7.800	6.140	4.610	3.105
3	23.185	24.765	26.185	27.750	.....	6.130	4.600	3.060
4	23.190	24.780	26.200	27.765	.....	6.130	4.600	3.050
5	23.205	24.785	26.205	27.775	.....	6.130	4.605	3.060
6	23.215	24.795	26.206	27.775	7.365	6.140	4.620	3.060
7	23.215	24.795	26.205	27.775	7.365	6.140	4.620	3.060
8	23.225	24.795	26.215	27.780	7.365	6.145	4.620	3.065
9	23.220	24.795	26.200	27.775	7.360	6.140	4.620	3.060
10	23.225	24.795	26.205	27.780	7.570	6.215	4.620	3.120

In order to see what effect an error in F_Y would have, F_Y was varied by ± 0.125 (i.e. one half gap so that some sparks appear in the wrong gap) and the newly calculated dipion mass compared with the old for each event. The mass differences had a standard deviation of less than one MeV/c^2 and 99% of the events had a difference of less than ± 5 MeV/c^2. Thus, if one knows the actual X coordinates of the center of each spark chamber X_0, he will have the relationship for converting X_M, Y_M to X actual, i.e.

$$X = \sin\theta^* \, (F_X - X_M) \mp \cos\theta^* \, (Y_M - F_Y) + X_0.$$

The values of X_0 for each chamber were determined using measurements made on the spark chambers with a milling machine and from the top

view. They were:

CHAMBER NUMBER	X_0
1	8.5075
2	12.7525
3	17.0225
4	21.2925
5	25.5425
6	29.7125
7	34.4950
8	38.9525

The effect of X_0 was not tested since the value of X from the top view is used and so X_0 does not enter into the calculation except in determining which gap the spark was in.

A word in note: From the two tables above, one can see that most chambers have relatively constant rotation angles and F_Y's from section to section. The exception is chamber five. There are two reasons for this. First, chamber five failed and had to be replaced, thus creating a major change. Second, for a part of the time chamber five's mirror was not properly seated on its mount, resulting in an anomously large rotation, etc.

From this rotation about the approximate center of the spark chamber image we have a rough relation for the actual Z coordinate:

$$Z = \cos\theta^* (F_X - X_M) \pm \sin\theta^* (Y_M - F_Y).$$

The plus sign is for chambers one through four, and the minus sign is for chambers five through eight.

(3) In order to refine this relation, a fit is made to particle trajectories (i.e. helices and straight lines) and the fiducials by adjusting additive constants to the Z-value of the coordinates in each chamber. These additive constants, AD, are constrained so that the average beam slope in the XZ plane is zero $\pm$ 5 milradians and the beam's average Z value is zero inches. The following table lists this refinement to F_X.

SECTION NUMBER	CHAMBER NUMBER							
	1	2	3	4	5	6	7	8
1	0.056	-0.085	0.002	-0.057	-0.024	0.113	0.003	-0.006
2	0.077	-0.075	0.008	-0.054	-0.019	0.116	0.005	-0.003
3	0.079	-0.073	0.011	-0.051	.....	0.134	0.008	-0.010
4	0.095	-0.083	0.011	-0.045	.....	0.128	0.008	-0.007
5	0.052	-0.081	0.010	-0.048	.....	0.131	0.008	-0.007
6	0.057	-0.080	0.010	-0.048	-0.042	0.132	0.006	-0.007
7	0.059	-0.076	0.014	-0.038	-0.076	0.122	0.007	0.001
8	0.057	-0.075	0.015	-0.039	-0.078	0.120	0.009	0.002
9	0.041	-0.077	0.016	-0.037	-0.078	0.120	0.009	0.001
10	0.061	-0.079	0.015	-0.036	-0.073	0.117	0.007	0.002

A liberal estimate of the error in this constant is $\pm$ 0.005"

A check was also made to see the effect of an error. Here the

values were staggered by ± 1.0", giving a mass difference spectrum with a standard deviation of ± 3 MeV/c^2. When a stagger of ± 0.25" was used, the standard deviation was less than one MeV/c^2 and 90% of the events had dipion masses within ± 5 MeV/c^2.

(4) The deviation of the reconstructed measured spark locations and the best least-square trajectories are then plotted as ΔZ vs X, Y, Z for each chamber (also for each fiducial).

ΔZ(mils)   e.g. Chamber 6 Section VIII
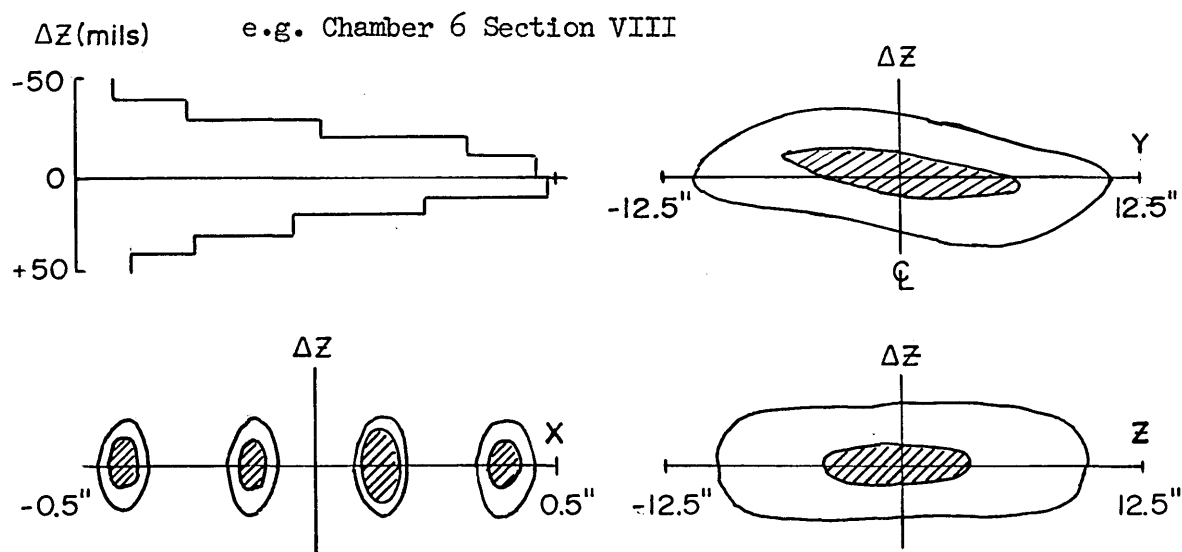
This allows observation of whether corrections are needed for X, Y, or Z dependence. Thus far it has not been thought necessary to make further corrections.

In summary, the relations connecting X_M, Y_M the measured side view coordinates, to the actual coordinates were:

$$X = \sin\theta^* (F_X - X_M) \mp \cos\theta^* (Y_M - F_Y) + X_0$$

$$Z = \cos\theta^* (F_X - X_M) \pm \sin\theta^* (Y_M - F_Y) + AD.$$

Beam Chamber Constants

Side View

Plan View
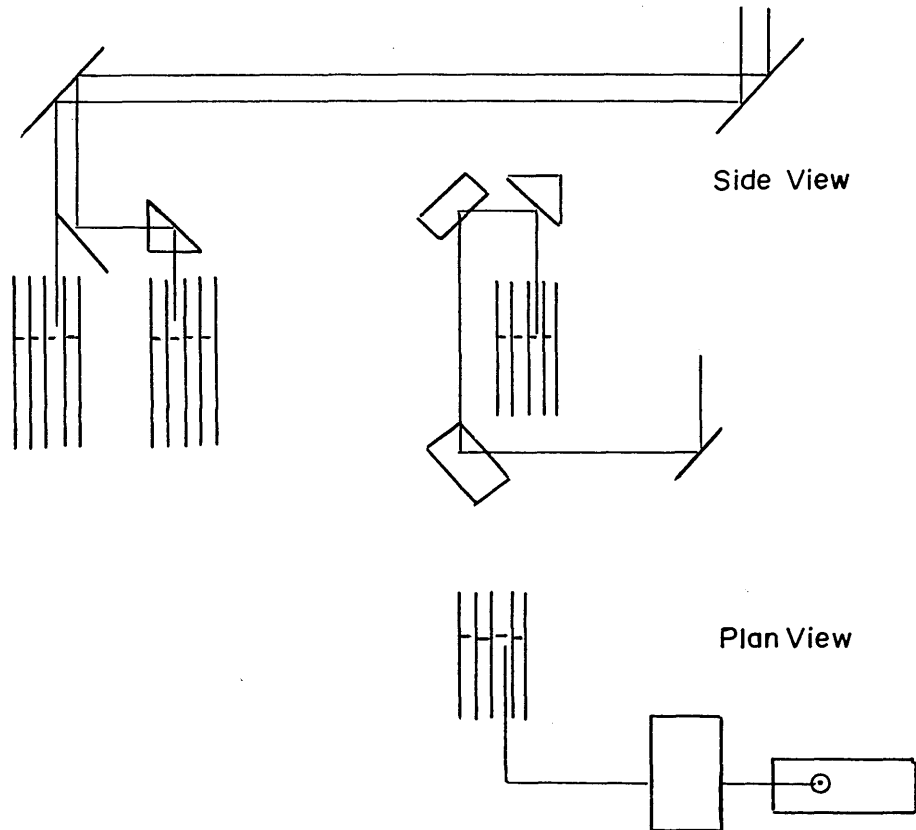
In the calculation of the beam chamber constants

(1) all mirrors are assumed to be plane surfaces

(2) only vertical light is accepted by the external optics.

The optics was aligned with the following relationship in mind:

RELATION	BEAM CHAMBER
$X_U = X_{UM} + X_{UO}$	Upstream
$X_M = X_{MM} + X_{MO}$	Middle
$X_{BT} = X_{BTM} + X_{BTO}$	Main Top View
$X_{BS} = Y_{BSM} + X_{BSO}$	Main Side View

where X_{UO}, Y_{MO}, X_{BO}, X_{BTO}, X_{BSO}, are constants. (See the section on the beam.)

There was also a tilted mirror under the upstream beam chamber to provide rough information on the height of the beam. The mirror was set up to be a $6°$ tilted mirror. Thus, one should have had

$$Z = 5.5 \times (Y_{IM} - Y_M) + (Y_M - 2.5)/11.0 - 3.0.$$

The result was

$$Z = 7.0 *(Y_I - Y_M) + (Y_M - 5.0)/14.0 - 3.0.$$

This was because the two other mirrors were not aligned properly with respect to the tilted mirror.

APPENDIX B

Requirements on raw data as encoded by Measuring Staff

An event is encoded on Hydel encoding machines. In measuring an event, first three (or if only two present then two) fiducial lights are measured, then the beam spark locations, next each track of the vee in the top view in succession, and finally each track in the side view in the same order as the top view. This usually requires about twelve IBM punch cards.

The following checks are made:

(1) Each card in an event must have

    (a) the same event number as the other cards

    (b) the same roll number

    (c) The first card must have sequence number 1 and each succeeding card must have the proper sequence number.

(2) The separation of the fiducials is checked to 1/4 % of total separation for three possible distances (or one distance for two fiducials).

(3) Each track of the vee is checked to see if it has more than eight sparks in it, in order to assure that sparks were measured in at least three chambers.

(4) In the top view, a correction is made to chamber seven spark locations and a circle is fitted to each track. Then a correction is made of E cross B drift. The correction takes on the form of mean square distance of the sparks to the best fitted circle. After

this treatment, the root mean square distance is required to be less than 50 mils. The reason a constant value is not used for the E cross B drift is that there was a fair amount of jitter in the firing time of spark chambers after the event had occurred.

(5) Corrections are made to the side view spark images and then a helix is fit with the side view and top view parameters. The root mean square distance of the side view spark images to the fitted curve is required to be less than 70 mils and the maximum must be less than 140 mils.

(6) There is also a check made to see if there are any spark images outside the chamber and mirror boundaries. A failure here is rare and is usually due to film slippage from loss of hold-down vacuum on the film.

Acknowledgements

I would like to thank Professor Frisch for his help and guidance during my research.

I thank Professor Glauber for taking the time to offer his advice and suggestions.

I would also like to thank my partners O. Fackler, J. Martin, and L. Sompayrac for all the work they have done which has greatly aided my efforts.

To my wife I express thanks for her understanding and assistance especially during the writing of this thesis.

Thank you to all the other people who have been so helpful.

Biographical Note

George Fitzgerald Smoot III was born in Yukon, Florida,
on February 20, 1945. He attended public schools in Alabama,
Alaska, and Ohio. He received the bachelor's degree in physics
and mathematics from the Massachusetts Institute of Technology
in 1966.